

Community Detection on Networks with Ricci Flow

Chien-Chun Ni¹, Yu-Yao Lin², Feng Luo³, and Jie Gao^{4,*}

¹Yahoo! Research, Sunnyvale, CA, USA

²Intel Corp., Hillsboro, OR, USA

³Rutgers University, New Brunswick, NJ, USA

⁴Stony Brook University, Stony Brook, NY, USA

*jgao@cs.stonybrook.edu

ABSTRACT

Many complex networks in the real world have community structures – groups of well-connected nodes with important functional roles. It has been well recognized that the identification of communities bears numerous practical applications. While existing approaches mainly apply statistical or graph theoretical/combinatorial methods for community detection, in this paper, we present a novel geometric approach which enables us to borrow powerful classical geometric methods and properties. By considering networks as geometric objects and communities in a network as a geometric decomposition, we apply curvature and discrete Ricci flow, which have been used to decompose smooth manifolds with astonishing successes in mathematics, to break down communities in networks. We tested our method on networks with ground-truth community structures, and experimentally confirmed the effectiveness of this geometric approach.

1 Introduction

Complex networks have been used to model connections of elements in many different fields such as social networks, biology, and biochemistry (protein-protein networks [1], metabolic networks, and gene networks), and computer science (P2P, the Internet). It has been widely recognized that many of real world networks have community structures – nodes in the same community are densely connected while nodes from different communities are sparsely connected. Recognition of community structures brings out important functional components and plays an important role in supporting processes on networks such as contagions of diseases, information or behaviors. Many algorithms have been developed to identify and separate communities in the literature [2, 3, 4, 5, 6, 7, 8, 9, 10, 11].

Most current works on community detection try to recognize dense clusters in a graph: by randomized algorithms such as label propagation [12] or random walks [13]; by optimized centrality such as betweenness centrality [14]; or by considering notions such as modularity [15]: the fraction of edges that fall within the given groups minus the expected fraction if edges were distributed uniformly at random (while still respecting the degree distribution). The viewpoint of modularity could be considered as a statistical measure of non-uniformity of the network.

Unlike existing methods, our work explores a new path connecting community detection and geometry. We consider community structure as a geometric phenomenon and use geometric methods to identify communities in a network. The motivation comes from the classical topological connected sum decomposition of 3-manifolds. The groundbreaking work of Hamilton and Perelman [16, 17] shows that the connected sum decomposition can be detected by the geometric Ricci flow. By considering a network as a discrete counterpart of a manifold and connected sum components as communities, we introduce a discrete Ricci flow on networks for identifying communities in a network.

The Ricci flow approach is based on the geometric notion of curvature, introduced by F. Gauss and B. Riemann over 150 years ago, which describes quantitatively how spaces are bent at each point [18]. In classical geometry, regions in a space with large positive curvature tend to be more densely packed than regions of negative curvature. To locate these regions of large curvature, in a seminal work in 1982, Hamilton [16] introduced a curvature guided diffusion process, called the Ricci flow, that deforms the space in a way formally analogous to the diffusion of heat. Under the Ricci flow, regions in a space of large positive curvature shrink to points whereas regions of very negative curvature spread out. In this paper, we observed that communities in networks resemble regions in Riemannian manifolds of large positive curvature. By applying the discrete Ricci flow on networks as the classic Ricci flow on manifolds, we are able to detect

community structures in networks.

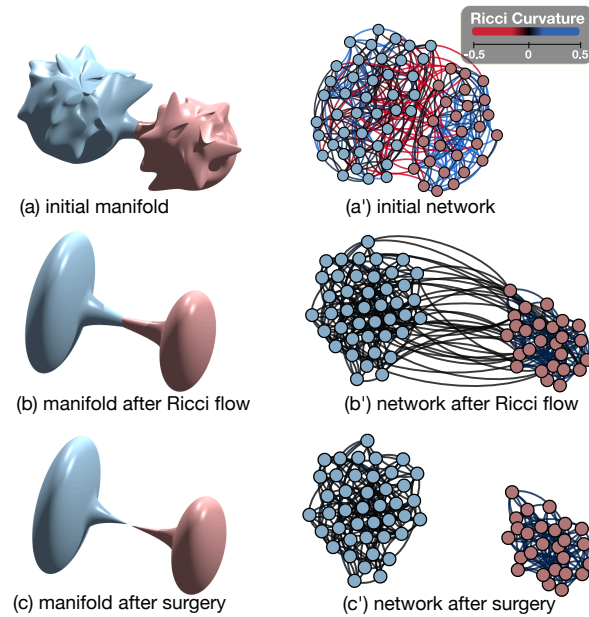


Figure 1. An illustration of Ricci flow on a manifold and a network. Ricci flow captures the large positive curvature regions in the manifold as well as communities in the network. The formation of singularities in the Ricci flow is illustrated by (b, c). The analog in (b', c') in the discrete Ricci flow decomposes the network into communities.

Figure 1 illustrates this key observation. In the left column, the Ricci flow deforms a Riemannian manifold (Figure 1(a)) gradually and develops a neck pinching singularity (Figure 1(b)). By removing the singularity, the manifold is decomposed into sub-regions of positive curvature (Figure 1(c)). In the right column, the discrete Ricci flow on a metric graph (Figure 1(a')) stretches edges of large negative Ricci curvature and shrinks edges of large positive Ricci curvature over time (Figure 1(b')). By removing the edges of weight greater than a threshold value, we recover subgraphs of large Ricci curvature representing communities (Figure 1(c')).

1.1 Our Contribution

To carry out the discretization process, we start from the recent important work of Y. Ollivier [19, 20, 21] which introduced Ricci curvature on metric measure spaces by using the optimal transport theory. Ollivier's definition for metric graphs assigns a probability measure to each node and the Ricci curvature of an edge is related to the optimal transportation cost between two probability measures defined on the vertices of the edge. Various definitions of Ricci curvatures on networks have been used in graph analysis for applications such as anomaly detection, detection of backbone edges or cancer related proteins [22, 23, 24, 25, 26, 27, 28, 29, 30].

Motivated by Hamilton's Ricci flow, we introduce an algorithm, called discrete Ricci flow on networks, for detecting community structures. The discrete Ricci flow is defined on weighted graphs and deforms edge weights as time progresses: edges of large positive Ricci curvature (i.e., sparsely traveled edges) will shrink and edges of very negative Ricci curvature (i.e., heavily traveled edges) will be stretched. By iterating the Ricci flow process, we are able to identify heavily traveled edges and thus find communities.

Figure 2 illustrates how discrete Ricci flow detects communities on the Zachary's Karate club graph. In this graph, individuals in the same club are represented as nodes of the same color, and friendship ties between two individuals are represented as edges with weights equal to 1. With discrete Ricci flow algorithm, the edge weights evolve such that the community structure can be easily detected by removing edges that are stretched greater than a threshold. Figure 3 shows another example of communities on a Facebook ego graph. We have also tested our Ricci flow algorithms on many of the real-world networks with ground-truth communities and artificial networks, and shown competitive accuracy results with other community detection algorithms using various statistical methods or physics models.

We applied the discrete Ricci flow method on artificial networks generated by the stochastic block model (SBM) [11], the Lancichinetti-Fortunato-Radicchi (LFR) benchmark graph [32] and the emergent geometrical network model [33, 34]

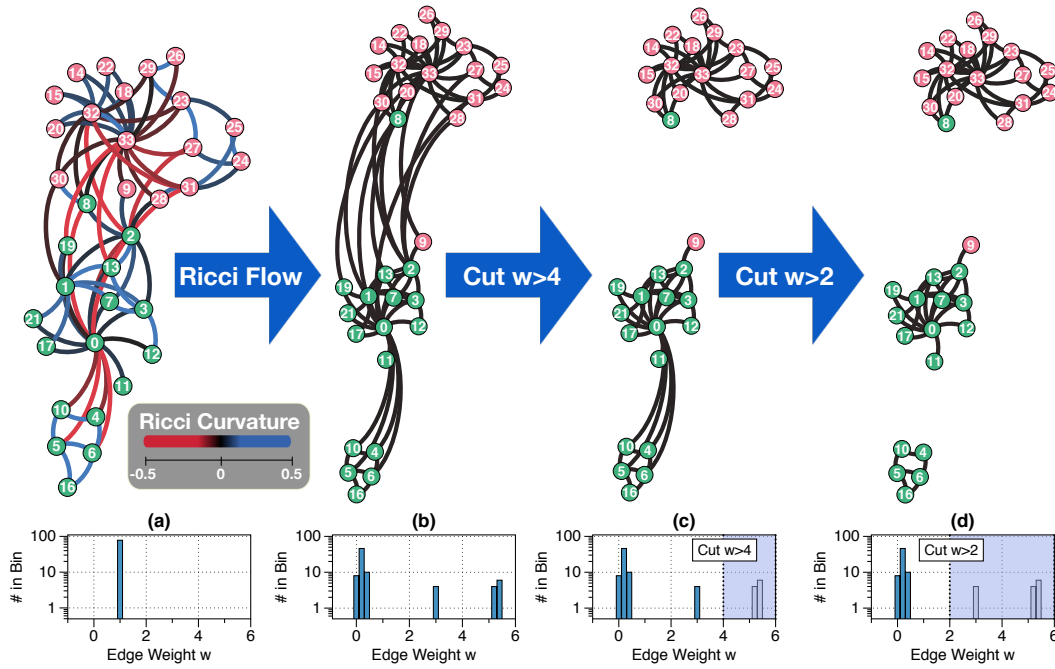


Figure 2. Ricci flow for community detection on the Karate club graph generated by Gephi’s ForceAtlas2 layout[31]. (a): The Karate club graph with edge weight 1 on all edges. Different colors of vertices represent different communities. The colors of edges represent the Ricci curvature on the edges. Notice that most edges between communities are negatively curved. (b): The same graph after 100 Ricci flow iterations. Ricci flow adjusts the edge weights so that the edge Ricci curvatures are the same everywhere; the intra-community edges shrink; the inter-community edges are stretched. (c) By removing all edges with weight greater than 4, we acquire a partitioning of the graph with two communities. (d) By removing all edges with weight greater than 2, we obtain three communities.

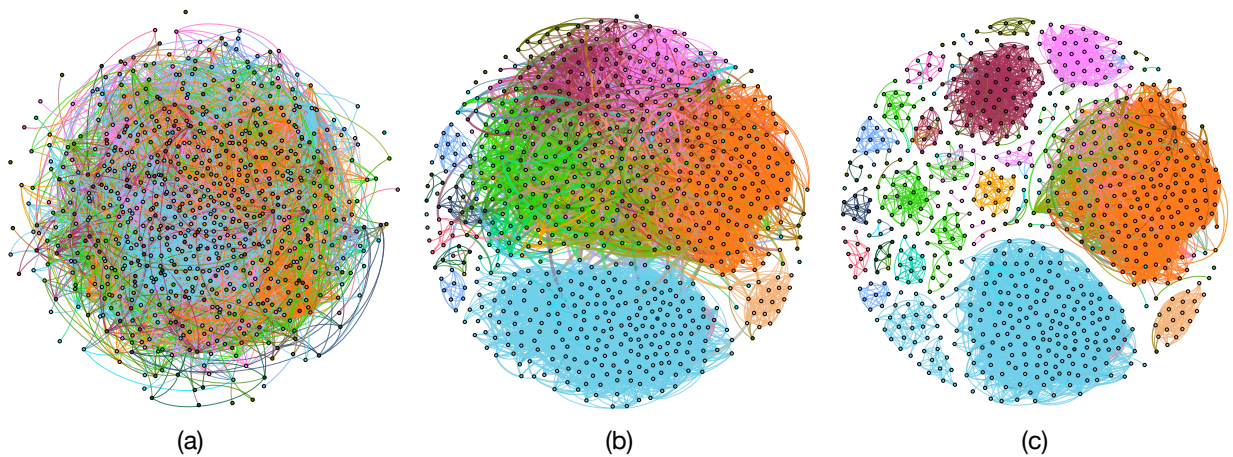


Figure 3. (a) A Facebook ego network of one user with 792 friends and 14025 edges generated by Gephi’s Fruchterman Reingold layout[31]. The colors represent 24 different friend circles (communities) hand labeled by the user. (b) By the Ricci flow process of 20 iterations, the weights of inter-community edges are increased (thick edges in the figure) while the weights of intra-community edges gradually shrink to 0 (thin edges in the figure). (c) By removing the inter-community edges with high weights, the communities are clearly detected.

(GNet). We choose Adjusted Rand Index (ARI) [35] as a quality measure for the clustering accuracy. The proposed discrete Ricci flow method is shown to provide nearly perfect clustering result when community structures exist. Also, extensive comparison tests on real networks with ground-truth communities show that our algorithm is competitive with previously proposed ones. Similar results have been observed with other metrics of clustering accuracy such as modularity.

Our work of Ricci curvature on networks is built on our previous works [22, 30] and is also inspired by the important works of E. Saucan and J. Jost *et al.* in [23, 27, 36, 37]. In these works, they systematically introduced and investigated various discrete curvatures for complex networks. The comparative analysis of Forman and Ollivier Ricci curvature on benchmark datasets of complex networks and real-world networks was also carried out. Their numerical results show a striking fact that these two completely different discretizations of the Ricci curvatures are highly correlated in many networks.

1.2 Related Work

Ricci curvature on general spaces without Riemannian structures has been recently studied, in the work of Ollivier [19, 20] on Markov chains, and Bakry and Emery [38], Lott, Villani [21], Bonciocat and Sturm [39, 40] on general metric spaces. Ricci curvature based on optimal transportation theory, proposed by Ollivier (Ollivier-Ricci curvature) [19, 20], has become a popular topic and been applied in various fields – for distinguishing cancer-related genes from normal genes [28], for studying financial market fragility [29], for understanding phylogenetic trees [26], and for detecting network backbone and congestion [22, 25, 41]. In [42], Pal *et al.* proposed to use Jaccard coefficients for a proxy for Ollivier-Ricci Curvature. Besides, discrete Ricci curvature has also been defined on cell complexes, proposed by Forman [43] (Forman curvature or Forman-Ricci curvature). Forman curvature is based on graph Laplacian. It is easier and faster to compute than Ollivier-Ricci curvature, but is less geometrical. It is more suitable for large scale network analysis [23, 24, 44, 45] and image processing [46]. We have also experimented with Forman curvature for community detection. The results were less satisfying. So here we focus on Ollivier-Ricci curvature.

Unlike discrete Ricci curvature, discrete Ricci flow has not been studied as much. Chow and Luo introduced the first discrete Ricci flow on surfaces [47]. In [44], Weber *et al.* suggested applying Forman-Ricci flow for anomaly detection in the complex network. In [30], Ni *et al.* used the Ollivier-Ricci curvature flow to compute the Ricci flow metric as edge weights for the problem of network alignment (noisy graph matching).

Community detection is a well-studied topic in social network analysis [2, 3, 6, 48, 49, 50, 51, 52], and protein-protein interaction networks [1, 53]. There are a few main ideas. One family of algorithms iteratively remove edges of high ‘centrality’, for example, the edge betweenness centrality as suggested in [14] by Girvan and Newman. The other idea is to use modularity (introduced by Newman and Clauset *et al.* [4, 7]), which measures the strength of division of a graph into clusters, as the objective of optimization. But methods using modularity suffer from a resolution limit and cannot detect small communities. A geometric extension, named Laplacian modularity, is also suggested with the help of Gauss’s law in [5]. Another family of algorithms borrows intuitions from other fields. In [54], a spin glass approach uses the Potts model from statistical physics: every node (particle) is assigned one of c spin states (communities); edges between nodes model the interaction of the particles. The community structure of the network is understood as the spin configuration that minimizes the energy of the spin glass. In [12], Raghavan *et al.* proposed a non-deterministic label propagation algorithm for large networks. In the initial stage, the algorithm randomly assigns each node in the graph one of c labels. Each node then changes its label to the most popular label among its neighbors. Infomap [13] uses an information theoretic approach. A group of nodes for which information flows quickly shall be in the same community. The information flow is approximated by random walks and succinctly summarized by network coding.

Taking a geometric view of complex networks is an emerging trend, as shown in a number of recent work. For example, the community structures were used as a coarse version of its embedding in a hidden space with hyperbolic geometry [55]. Topological data analysis, a typical geometric approach for data analysis, has been applied for analyzing complex systems [56].

2 Classical theory of Ricci curvature, Optimal transport and the Ricci flow

In this section, we briefly recall the basic notation of Ricci curvature in Riemannian geometry, Ollivier’s work on generalizing Ricci curvature to metric measure spaces through optimal transport, and the Ricci flow. Their discrete and computational counterparts are addressed in Section 3.

2.1 Sectional and Ricci curvature

One of the central themes in modern geometry is the notion of curvature which quantitatively measures how space is curved. It was introduced by Gauss and Riemann. For a surface in the 3-dimensional Euclidean space, the *Gaussian curvature* at a point is defined as the signed area distortion of the Gauss map sending a point on the surface to its unit normal vector. For instance, a plane has zero curvature, a sphere has positive curvature and a hyperboloid of one sheet has negative curvature (Figure 4). Gauss showed that curvatures depend only on the induced Riemannian metric on the surface, i.e., independent of how a surface is embedded in the 3-dimensional space.

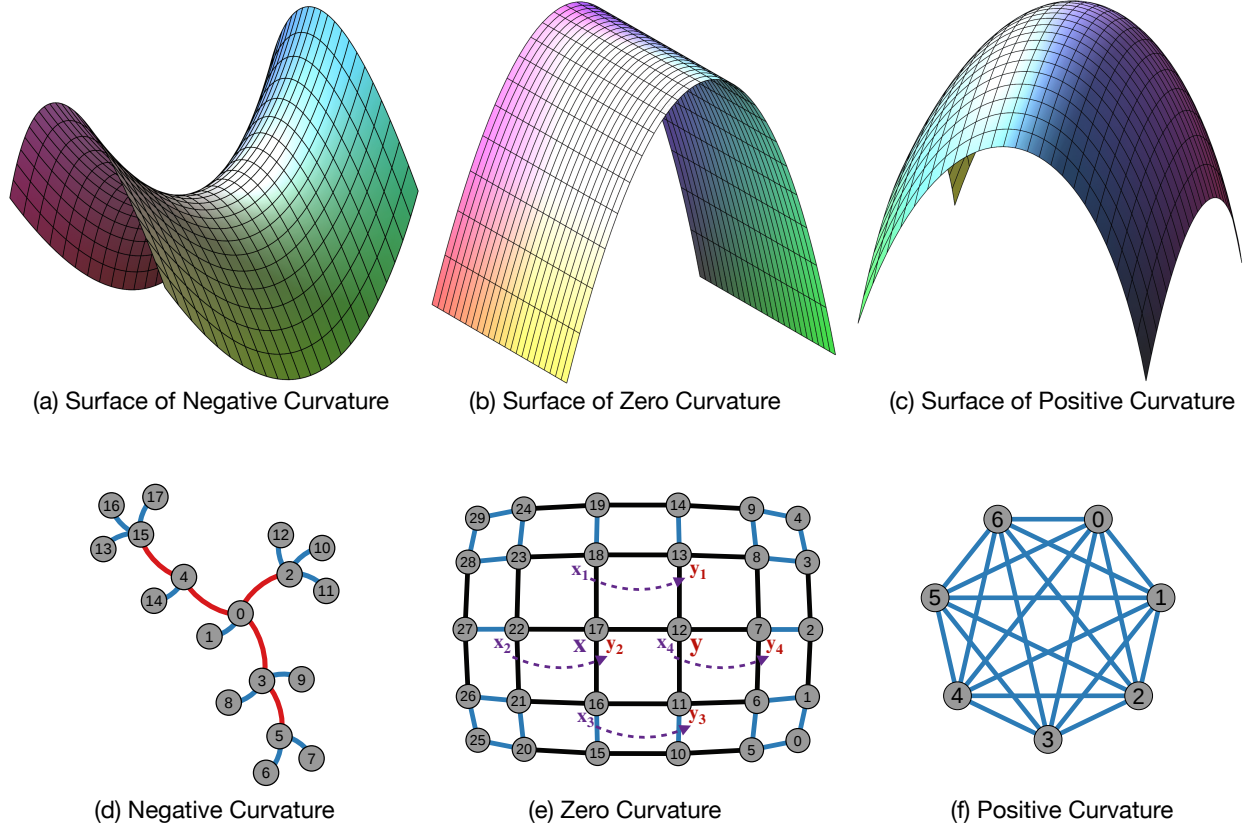


Figure 4. Examples of Ricci curvature on manifolds and graphs. In (a)-(c), manifolds with negative, zero, and positive curvatures are shown. In (d)-(f), all edges have weight of 1. (d) A tree graph with negative curvature everywhere, except the edges of the leaf nodes. (e) A (infinitely sized) grid graph with all edges of zero curvature. The cost of moving $m_x = \{x, x_1, x_2, x_3, x_4\}$ to $m_y = \{y, y_1, y_2, y_3, y_4\}$ is equal to $d(x, y)$ (f) A complete graph with all edges of positive curvature.

For a Riemannian manifold (M, g) , Riemann's *sectional curvature* assigns a scalar to each 2-dimensional linear subspace P in the tangent space at a point p of M . This scalar is equal to the Gaussian curvature of the image of P under the exponential map at p . A positive sectional curvature space tends to have a small diameter and is geometrically crowded (e.g., a sphere). In contrast, a negative sectional curvature closed Riemannian manifold has an infinite fundamental group, a contractible universal cover, and is geometrically spreading out like a tree in large scale. Thus, a positively curved region behaves more like a 'community' than negatively curved regions. Similar to sectional curvature, the *Ricci curvature* assigns each unit tangent vector v at p a scalar which is the average of the sectional curvatures of planes containing v . Geometrically, Ricci curvature controls how fast the volume of a ball grows as a function of the radius. It also controls the volume of the overlap of two balls in terms of their radii and the distance between their centers. On the other hand, the volume of the overlap of two balls is directly related to the cost of transportation to move one ball to the other, i.e., a larger volume of overlap means less cost of moving one ball to the other. It shows that the Ricci curvature is related to optimal transportation. An explicit formula (Equation 1) that builds a bridge between them was worked out by Ollivier [19]. Through the formula, Ollivier defined the generalized Ricci curvature on metric measure spaces by the optimal transportation.

2.2 The optimal transportation and Ollivier's Ricci curvature.

The original optimal transport problem was proposed by G. Monge in 1781. The problem wants to minimize the transportation cost to move iron ores from different mines to a collection of factories which consume the iron ores. In Monge's setting, the problem can be mathematically formulated as follows. Let mines and factories as two probability spaces X and Y ; the amount of iron ores to be moved and consumed as two probability Borel measures μ and ν , we define the cost of transporting from location x to location y to be $c(x, y)$, where $c : X \times Y \rightarrow \mathbb{R}_{\geq 0}$. In general, the cost function c is usually taken to be the distance $d(x, y)$ if $X = Y$ and the cost of transportation per-unit distance is constant. A transportation $T : (X, \mu) \rightarrow (Y, \nu)$ is a measure preserving map. Monge's formulation of the optimal transportation problem is to find a transportation $T : X \rightarrow Y$ that realizes $\inf \{ \int_X c(x, T(x)) d\mu(x) \mid T: \text{transportation} \}$.

Monge's optimal transportation problem had a major breakthrough in 1930 when Kantorovich formulated the optimal transportation problem into a linear optimization problem. In his setting, Kantorovich replaces transportation maps T by probability measures γ on $X \times Y$ (called *transportation plans*) satisfying $\gamma(A \times Y) = \mu(A)$ and $\gamma(X \times B) = \nu(B)$ for all measurable subsets A and B . The goal is to find a transportation plan γ that attains the infimum cost

$$W(\mu, \nu) = \inf \left\{ \int_{X \times Y} c(x, y) d\gamma(x, y) \mid \gamma \in \Gamma(\mu, \nu) \right\},$$

where $\Gamma(\mu, \nu)$ denotes the collection of all possible transportation plans. If X is a metric space with distance function d and $X = Y$, the quantity $W(\mu, \nu)$ for $c(x, y) = d(x, y)$ is called the *Wasserstein distance* (or the earth mover's distance) between two probability measures μ, ν on X .

Wasserstein distance plays a crucial role in Ollivier's approach to Ricci curvature. In his observation [19], if (M^n, d) is an n -dimensional Riemannian manifold with Riemannian volume μ and fix $\varepsilon > 0$, let $m_x = \frac{\mu|_{B(x, \varepsilon)}}{\mu(B(x, \varepsilon))}$ be the probability measure associated to $x \in M$ where $B(x, \varepsilon)$ is the ball of radius ε at x . Then the Wasserstein distance $W(m_x, m_y) = (1 - k(x, y))d(x, y)$, where

$$k(x, y) = \frac{\varepsilon^2 \text{Ricci}(v, v)}{2(n+2)} + O(\varepsilon^3 + \varepsilon^2 d(x, y)) \quad (1)$$

and v is the tangent vector at x of the geodesic xy . This shows that Ricci curvature can be defined for general metric spaces with measures. Given a metric space (X, d) equipped with a probability measure m_x for each $x \in X$, the Ollivier's Ricci curvature along the path xy is defined to be

$$\kappa_{xy} = 1 - \frac{W(m_x, m_y)}{d(x, y)}, \quad (2)$$

where $W(m_x, m_y)$ is the Wasserstein distance with respect to $c(x, y) = d(x, y)$.

2.3 The Ricci flow

The Ricci flow, introduced by Richard S. Hamilton in 1981 [16], deforms the metric of a Riemannian manifold in a way formally analogous to the diffusion of heat, smoothing out irregularities in the metric. The Ricci flow has been one of the most powerful tools for solving geometric problems in the past forty years. The flow exhibits many similarities with the heat equation.

Suppose a Riemannian metric g_{ij} is given on a manifold M so that its Ricci curvature is R_{ij} . Hamilton's Ricci flow is the following second-order nonlinear partial differential equation on symmetric $(0, 2)$ -tensors:

$$\frac{\partial}{\partial t} g_{ij} = -2R_{ij}.$$

A solution to the Ricci flow is a one-parameter family of metrics $g_{ij}(t)$ on a smooth manifold M satisfying the above partial differential equation. One of the key properties of the Ricci flow is that the curvature evolves according to a nonlinear version of the heat equation. Thus the Ricci flow tends to smooth out irregularity of the curvature. Under the Ricci flow, regions in the manifold of positive sectional curvature tend to shrink and regions of negative sectional curvature tend to expand and spread out. Singularities usually occur while deforming a Riemannian 3-manifold through the Ricci flow. They appear in a small neighborhood of a surface in the 3-manifold. By removing the singularities (i.e., surfaces) and redefining the Ricci flow on the remaining pieces, one produces the Ricci flow with surgery on the manifold. Figure 1 (b) and (c) illustrate the formation of a singularity and the 'surgery' operation. The ground-breaking

work of Perelman [17] shows that the Ricci flow with surgery captures the geometric decomposition of the 3-manifold. It solves the Geometrization Conjecture of Thurston and geometrically classifies all 3-manifolds.

Ricci flow enables a better understanding of the evolution and community structure of networks. In our heuristic thinking, a network is analogous to a discretization of high dimensional manifold (say a 3-manifold) and communities in the network are analogous to the components in the geometric decomposition of the 3-manifold. Since Perelman's work [17] proved that the Ricci flow is able to predict geometric components of a 3-manifold, it suggests that a discrete Ricci flow on the network should be able to detect the community structure. Just like in Hamilton-Perelman's work on Ricci flow, the cutoff number of iterations and threshold value for surgery in Ricci flow depend on individual networks.

3 Theory and Algorithms on Discrete Ollivier Ricci Flow

In this section, we introduce our discrete Ricci flow algorithm for community detection on the network. We started with the definition of Ricci curvature by Ollivier in Equation 2, for each node x on a metric graph $G = (V, E, w)$, we define a mass distribution m_x on x 's neighbor nodes. A discrete *transport plan* is a map $A : V \times V \rightarrow [0, 1]$ such that $A(u, v)$ is the amount of mass at vertex v to be moved to vertex u . It satisfies $\sum_{v' \in V} A(u, v') = m_x(u)$ and $\sum_{u' \in V} A(u', v) = m_y(v)$. The Wasserstein distance here $W(m_x, m_y)$ is defined as the minimum total weighted travel distance to move m_x to m_y , i.e., $W(m_x, m_y) = \inf\{\sum_{u,v \in V} A(u, v)d(u, v)\}$. The discrete Ricci curvature on a network edge $xy \in E$ is defined as

$$\kappa_{xy} = 1 - \frac{W(m_x, m_y)}{d(x, y)},$$

where $d(x, y)$ is the length of the shortest path between nodes x and y .

Under this definition, if two nodes x and y are from different communities, their neighbor nodes tend to have fewer common neighbors, hence the best way to move m_x from x 's neighbors to m_y in y 's neighbors is to travel along the edge xy . Because of this, the Wasserstein distance is necessarily larger than the length of xy , which leads to negative Ricci curvature. Alternatively, nodes within the same community tend to share neighbors or have shortcut between neighbors, thus have a Wasserstein distance no greater than $d(x, y)$. Therefore intra-community edges are mostly positively curved. See Figure 4 for examples of network edges of positive, zero and negative curvatures.

Note that the probability distribution m_x for $x \in V$ needs to be specified. In previous work [57], the probability distribution is uniform on x 's neighbors. In this paper, we suggest a more general family of probability distributions $m_x^{\alpha, p}$, with two parameters: $\alpha \in [0, 1]$ and power $p \geq 0$:

$$m_x^{\alpha, p}(x_i) = \begin{cases} \alpha & \text{if } x_i = x \\ \frac{1-\alpha}{C} \cdot \exp(-d(x, x_i)^p) & \text{if } x_i \in \pi(x) \\ 0 & \text{otherwise} \end{cases}$$

Here $C = \sum_{x_i \in \pi(x)} \exp(-d(x, x_i)^p)$ is a normalization factor and $\pi(x)$ is the set of neighbors of x . The parameter α determines the probability to remain at x . The power parameter p determines how much we want to discount the neighbor x_i of x with respect to the weight $d(x, x_i)$. When $p = 0$, the probability measure is uniform on all neighbors of x as suggest in [57]. For a large p , the neighbors that are far away from x are aggressively discounted.

The discrete Ricci flow algorithm on a network is an evolving process. In each iteration, we update all edge weights simultaneously by the following flow process:

$$w_{xy}^{(i+1)} = d^{(i)}(x, y) - \kappa_{xy}^{(i)} \cdot d^{(i)}(x, y),$$

where $w_{xy}^{(i)}$ is the weight of the edge xy at the i -th iteration, and $\kappa_{xy}^{(i)}$ is the Ricci curvature at the edge xy at the i -th iteration, and $d^{(i)}(x, y)$ is the shortest path distance on the graph induced by the weights $w_{xy}^{(i)}$. Initially $w_{xy}^{(0)} = w_{xy}$ and $d_{xy}^{(0)} = d_{xy}$. The detailed algorithm is presented in supplementary information.

This discrete Ricci flow process expands negatively curved edges and shrinks positively curved edges. Eventually, nodes connected by intra-community edges are condensed and inter-community edges are stretched. By this effect, a simple thresholding procedure can easily separate different communities. This is termed network 'surgery' when edges of large weights (likely inter-community edges) are removed after several Ricci flow iterations (usually 10 to 15 iterations). See Figure 2 as an example for the surgery process. For networks with hierarchical community structures, we may perform multiple rounds of network surgery and Ricci flow to fully separate communities at different scales.

4 Results

4.1 Theoretical Results

We can prove rigorously that the Ollivier-Ricci flow with respect to the specific choice of $\alpha = 0$ and $p = 0$ can successfully detect community structure for the following $G(a, b)$ family of graphs (Please refer to supplementary information for further detail). Take the complete graph on $b + 1$ vertices p_1, \dots, p_{b+1} and $b + 1$ complete graphs C_1, \dots, C_{b+1} on $a + 1$ vertices. Take a vertex u_i from each C_i and identify u_i with p_i . The resulting graph is $G(a, b)$. For $a > b$, this is a highly symmetric graph with a clear community structure – each copy of C_i is a community and there are $b + 1$ of them. Between any two communities C_i, C_j , there is only one edge $u_i u_j$ joining them. This community structure can be detected by the Ollivier-Ricci flow with respect to the Ollivier-Ricci curvature K_0 corresponding to $\alpha = 0, p = 0$ in Section 3. More precisely, the Ollivier-Ricci curvature K_0 is associated with the probability distribution μ_x such that $\mu_x(y) = 1/d_x$ if y is adjacent to x and $\mu_x(y) = 0$ otherwise. In this case, we are able to compute explicitly the Ollivier-Ricci curvature at the n -th iteration of the Ricci flow and confirm how the weights of the network edges evolve over time.

Theorem 4.1. *The Ricci flow associated to the Olivier K_0 -Ricci curvature detects the community structure on $G(a, b)$ if $a > b \geq 2$, namely, the weight of the intra-community edges shrink asymptotically faster than the weight of the inter-community edges.*

Proof: Please refer to supplementary information. □

4.2 Experimental Results

In this section, we explain the model networks and real-world datasets used to evaluate the community detection accuracy of our method. For the model network, we tested the growing geometrical network model with emergent complex geometry (GNet), and two models that provides community labels: the standard and widely used stochastic block model (SBM), and the Lancichinetti-Fortunato-Radicch benchmark model (LFR) that generates graphs of power-law degree distributions. For real-world datasets, we picked 6 different community graphs that come with *ground-truth community* labels. More detailed experiments can be found in supplementary information.

4.2.1 Model Networks and Real World Datasets

Stochastic Block Model The *stochastic block model* (SBM) is a probabilistic graph model [11]. A graph following the stochastic block model has n vertices, which are partitioned into k communities. Two nodes within a community are connected with probability p_{intra} while two nodes in different communities are connected with probability p_{inter} , $p_{intra} > p_{inter}$.

Lancichinetti-Fortunato-Radicch Model The Lancichinetti-Fortunato-Radicch (LFR) benchmark [32] generates undirected unweighted networks with non-overlapping communities. The model produces networks with both degree and community size satisfying power-law distributions. This model is also commonly used to evaluate community detection algorithms [2].

Emergent Geometrical Network Model The emergent geometrical network model [33, 34] (GNet) describes a growing network with high clustering coefficient using the triadic closure property. It is observed to have non-trivial community structures. One version described in [34] could grow a geometric network. It is composed of the skeleton of a simplicial complex in which a set of 2-simplices are glued together properly. The generation of this model is controlled by the designated number m of 2-simplices glued along a 1-simplex (edge), and the probability p of connecting two nodes with hop distance 2.

Real World Datasets For real world datasets, we choose networks that provide ground truth communities from KONECT[58], UCI network data repository and Stanford Network Analysis Project [59]. The statistics of the real world datasets are summarized in Table 1. In the followings, we briefly describe the datasets.

- **Karate club network** The Karate club network dataset was collected from the members of a university karate club by Wayne Zachary in 1970s. The network is undirected in which nodes represent members of the club, and edges represent ties between two members. This dataset is generally used to find the two groups of people into which the karate club fission after a conflict between two faculties.

Table 1. Real World Dataset

Datasets	V	E	#Class	AvgDeg	CC	Diameter
Karate Club	34	78	2	4.5882	0.5706	5
Football	115	613	12	10.6608	0.4032	4
Polbooks	105	441	3	8.4000	0.4875	7
Polblogs	1222	16714	2	27.3552	0.3203	8
FB-Ego	792	14025	24	35.417	0.483	10
Email-EU-core	1005	16064	42	31.968	0.450	7

- *American college football network* The American college football network is a representation of the schedule of Division I games during the season Fall 2000 and was previously used for community detection by Girvan and Newman . Each node represents a football team and each edge indicates a game between two teams. The community structure of the network is given by partitioning the teams into 12 conferences. Games held between teams of the same conference are held more frequently than games played between different conferences.
- *Political books network* This is a network of books about US politics published around the time of the 2004 presidential election and sold by the online bookseller *Amazon.com*. Edges between books represent frequent co-purchasing of books by the same buyers.
- *Political blogs network* The 2004 U.S. Presidential Election was notably influenced by blogs. The political blogs network dataset was collected by Adamic and Glance in 2005. The posts published by either liberal or conservative bloggers are represented by nodes. Any two nodes are connected by an edge if one of them is cited by the other.
- *Ego-network from Facebook* The ego-network dataset consists of ‘friend circles’ of one anonymous user and his/her friends on Facebook. The network forms friend circles such as family members, high school friends or other friends that are ‘hand labeled’ by the user. To normalize the influence of users belongs to multiple circles, we treat the overlaid circle as a new circle.
- *Email-EU-core network* The Email-Eu-core network was formed by the email contacts between members of a large European research institution. The members are represented by nodes where any pair of nodes are connected by an edge if they have had contacts through e-mail. Each individual belongs to exactly one of 42 departments at the research institute.

4.2.2 Experimental Results

To evaluate the clustering accuracy of our algorithm, we tested the clustering result with two different metrics: Adjusted Rand Index (ARI) and modularity. ARI measures the accuracy of clustering result with the *ground truth* clustering. Modularity quantifies the strength of the community structure of a given graph without the need of ground-truth clustering.

Clustering Accuracies The Clustering accuracies of applying discrete Ricci flow for 50 iterations is shown in Figure 5. In Figure 5(a) and Figure 5(b), the parameters p_{inter}/p_{intra} of the SBM and μ of the LFR indicate the magnitude of community structure of the models respectively. In both models, higher parameter values in x -axis indicate weaker community structures. We choose the adjusted Rand index (ARI) [35] as the quality measure for the clustering accuracy compared with the ground truth, as shown in the vertical axes. The ARI score represents the agreement of partitioned node pairs in ground truth communities and clustered communities. The higher the ARI score is, the more accurate our detected communities are. The results of Ricci flow algorithm show robust detection of community structures that compares favorably with prior algorithms – with a sharp phase transition from nearly 100% accuracy for SBM models with $p_{inter}/p_{intra} = 0.5$ (almost all nodes separated correctly) to nearly 0% accuracy for models with $p_{inter}/p_{intra} = 0.55$ (meaning the non-existence of community structure). Similar results have been observed with modularity.

To remove the singularities generated during the Ricci flow, we applied the surgery which removed edges with weight greater than an intermediate cutoff threshold for every 5 iterations during the whole 50 iteration process. The clustering accuracy results under different accuracy metrics are shown in Figure 6. In Figure 6(a), when the (final)

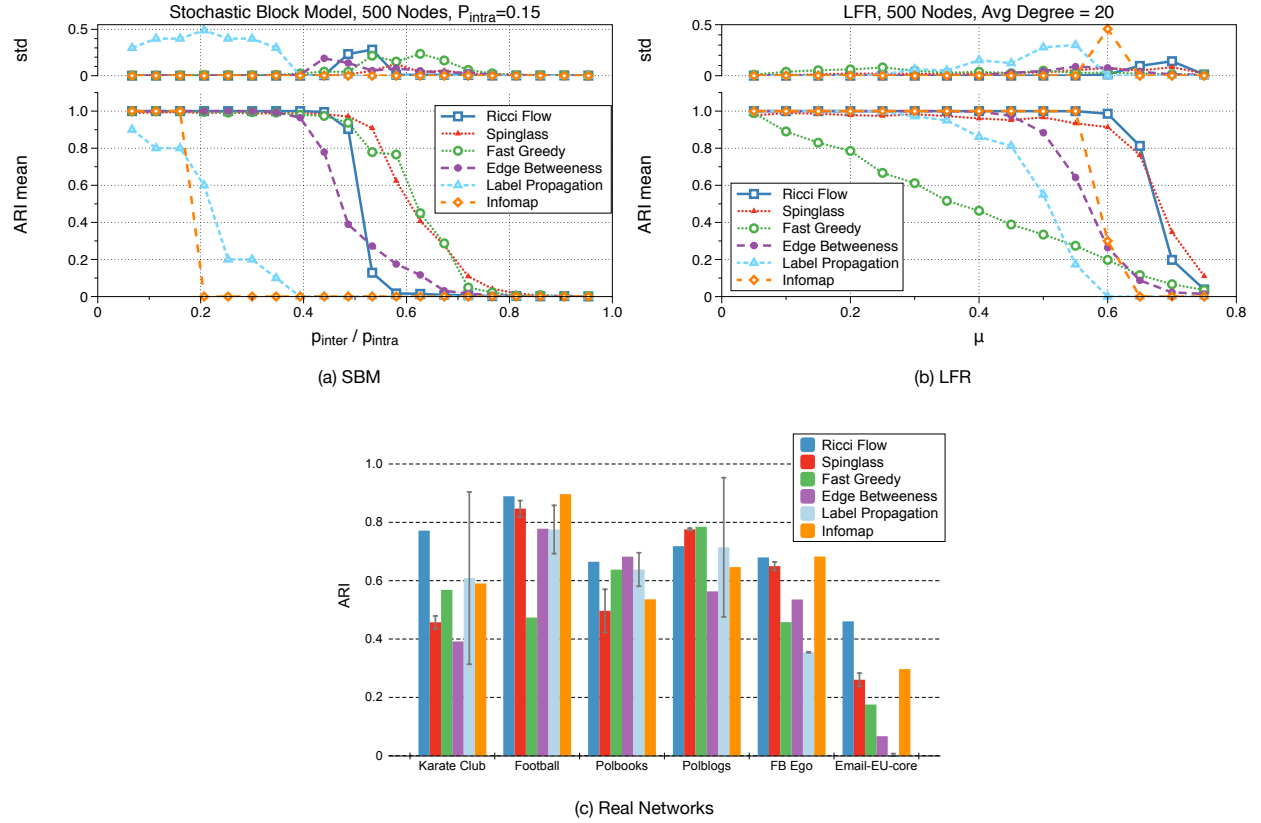


Figure 5. The accuracy of the Ricci flow method for community detection on model networks. The accuracy is measured by the adjust Rand index (ARI) and each data point is the average of 10 model graphs. In (a), we tested on the stochastic block model (SBM) with 500 nodes and two communities of the same size. A graph with low p_{inter}/p_{intra} ratio has more distinctive communities. Our method is shown to have perfect accuracy with $p_{inter}/p_{intra} < 0.5$. In (b), for Lancichinetti-Fortunato-Radicchi (LFR) Model, we set the graph to have 500 nodes, average degree of 20, with 38 communities. LFR can produce graphs with power-law degree distribution with communities of different sizes. The magnitude of community structure is controlled by μ , the ratio of inter-community edges with intra-community edges. Again, our method produces the best accuracy among all methods. In (c), for non-deterministic algorithm Spinglass and Label Propagation, the accuracy are averaged over 10 runs.

cutoff threshold is set between 1 and 0.47, we have a perfect clustering result of detecting all 30 communities, and this is correctly captured by ARI with the highest possible score 1.0. (In classical case of Hamilton-Perelman Ricci flow on 3-manifolds, the time to do surgery depends on individual manifolds) For modularity, the trend of capturing the perfect clustering accuracy result is similar to ARI (before the cutoff threshold 0.47), but its highest score occurs with a cutoff threshold of 0.275, which detected 290 communities. With this connection that ARI and modularity tend to capture the communities in the same trend, hence for networks without community labels such as GNet, a cutoff threshold is suggest to be when modularity first hits the plateau of the curve, for example with cutoff at 3.2 in Figure 6(b). This cutoff threshold also gives us a hint to detect hierarchical community structures. In Figure 7, layered community structures are revealed by applying different cutoff thresholds after 20 iterations of discrete Ricci flow processes.

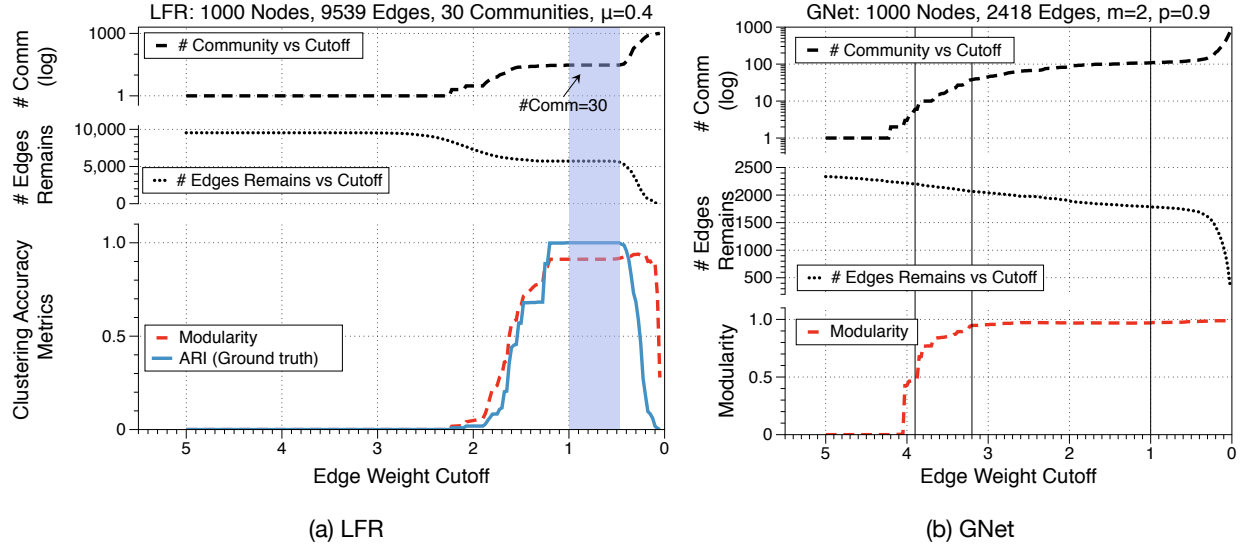


Figure 6. A comparison of clustering accuracy on an LFR graph after 50 iterations and GNet after 20 iterations of the Ricci flow with different final edge weight cutoff thresholds. In (a), with cutoff threshold set between 1 and 0.47 as the range highlighted in blue, we detected all communities correctly. In (b), we chose the cutoff threshold to be the turning point of modularity at $w = 3.2$ as the middle vertical line. To compare the communities detected with different cutoff thresholds, two extra cutoff $w = 3.9$ and $w = 1$ are added. The detected communities are shown in Figure 7.

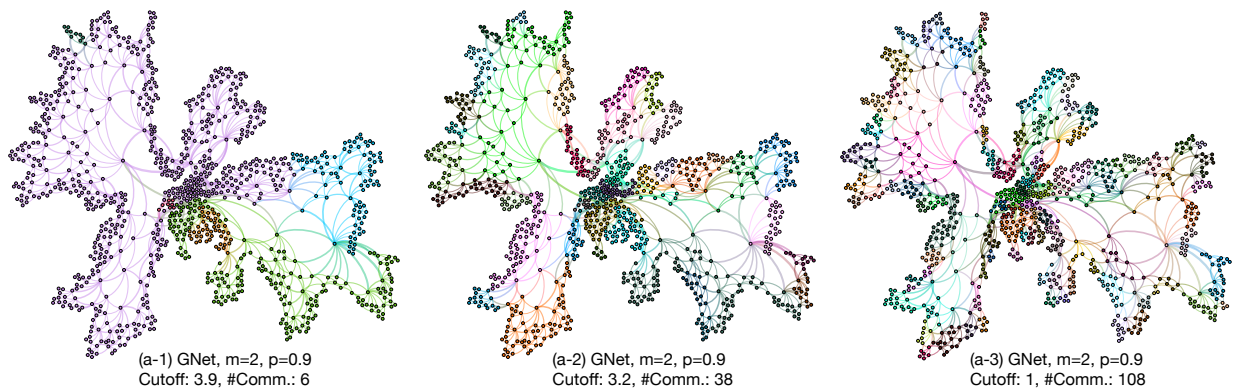


Figure 7. Illustrations of communities detected by discrete Ricci flow with three different cutoff weights of a GNet planar model with 1000 nodes, $m = 2$, and $p = 0.9$. With different cutoff thresholds (labeled as vertical lines in Figure 6(b)), we are able to detect communities in a hierarchical manner.

4.2.3 Comparison with Other Methods

We compared our result with the community detection algorithms such as Modularity based Fast Greedy algorithm [7], Label Propagation [12], Infomap [13], Spinglass [54], and Edge Betweenness [14] (by iGraph: <http://igraph.org/python/>) with Adjusted Rand Index (ARI) as the accuracy metric.

We first tested community detection algorithms on a simple graph model SBM with 500 nodes, 6800 edges and two even size communities in Figure 5(a). We fixed $P_{inter} = 0.15$ and tested the mixing ratio P_{intra}/P_{inter} from 0.1 to 0.9. For SBM, beside label propagation method and Infomap, most of the algorithms perform well when the mixing ratio is below 0.5.

For LFR graphs, Ricci flow and Spinglass outperform all other methods in our experiments (Figure 5(b)). Compared to the accuracy of 95% for Spinglass, Ricci flow is more stable with nearly perfect accuracy for most of the values of μ .

We also evaluated community detection algorithms on different real-world datasets. In Figure 5(c), Ricci flow shows competitive or better results in Karate club, Football, Polbooks, and Polblogs datasets.

One key factor of a community structure is the density of connections within communities, the community structure is stronger if nodes in one community are more densely connected. In Figure 8, we tested Ricci flow and spinglass on LFR graphs with different average degree settings. The results show that with a higher average degree (higher edge density within communities) both algorithms provide better clustering results.

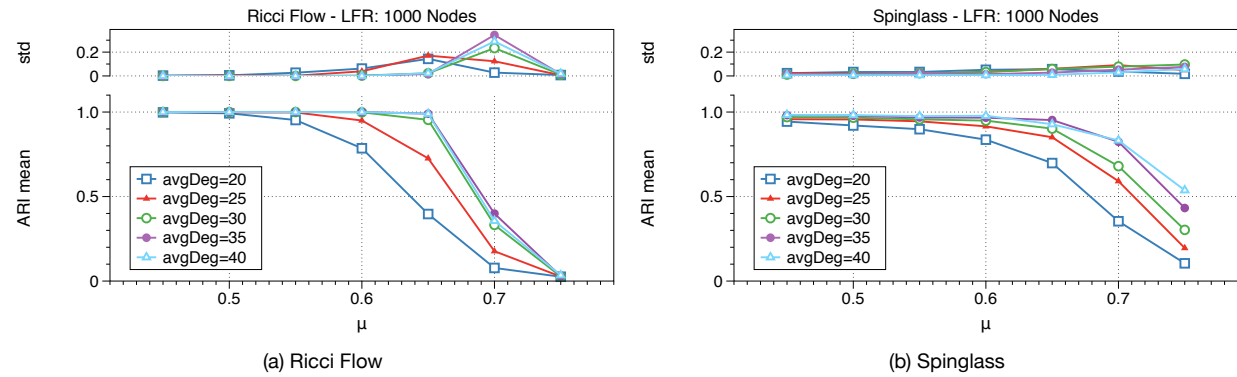


Figure 8. Ricci flow and spinglass algorithms on LFR graphs with different average node degrees. With a higher average degree which implies higher edge density within communities, both algorithms provide better clustering results.

5 Conclusion

In this paper, we have introduced geometric tools to investigate the community structures on complex networks. The basic idea is to consider networks as geometric objects and use the notion of curvature and curvature guided flow to decompose networks. In classical mathematics, Ricci curvature and Ricci flow are among the most important tools for analyzing and decomposing manifolds according to their geometric and topological properties. What is interesting is that the corresponding discrete counterparts are shown to be powerful for detecting community structures. Interesting future works include improving the theoretical understanding of discrete curvature on graphs and applying our methods for real-world applications.

Acknowledgement.

The authors would like to acknowledge support by NSF DMS 1737876, NSF DMS 1405106, NSF DMS 1811878, NSF FRG 1760527, NSF DMS-1737812, NSF CNS-1618391 and NSF CCF-1535900. We thank Xianfeng David Gu and Wujun Zhang for discussions.

Author Contributions.

All authors have contributed to the design of algorithms and writing of the article. Yu-Yao Lin and Chien-Chun Ni carried out implementation of the algorithm as well as evaluations under different models.

Competing interests

The authors declare no competing interests.

Data availability statement

The datasets generated during and/or analyzed during the current study are available from the corresponding author on reasonable request. Code for graph Ricci curvature and Ricci flow computation is available on github (<https://github.com/saibalmars/GraphRicciCurvature>).

Correspondence

Please send correspondences to Jie Gao, Department of Computer Science, Stony Brook University, Stony Brook, NY 11794. Email: jgao@cs.stonybrook.edu.

Supplementary Materials

A Theoretical foundation

We model a network as an unweighted graph $G = (V, E)$ with node set V and edge set E . The community detection problem on G is to find a collection of edges, called *inter-communities edges*, such that removing these edges from G produces a collection of connected subgraphs C_1, \dots, C_n , called *communities*, with the following properties (1) nodes in each community C_i are heavily connected by *intra-community edges* among themselves and (2) nodes in different communities are sparsely connected. It has been observed in many real-world networks (e.g., social, biological, the Internet) that communities exist. Detecting communities in a network has become an important and fundamental problem in complex networks with many applications. However, from a mathematical point of view, a precise and universally accepted definition of community structure is still lacking.

Our approach to define communities in a network uses the notion of Ricci curvature in geometry and the mathematical theory of optimal transport. Consider a graph G as a transportation network, edges between different communities are heavily traveled compared to edges within a community, since traffic prefers to take shortest paths whenever possible. Specifically, one can quantify the amount of traffic through an edge using the transportation cost from the optimal transportation theory.

We will use the following definitions and conventions. Two vertices (or nodes) $i, j \in V$ are adjacent, denoted by $i \sim j$, if they are the endpoints of an edge. In this case, we denote the edge by ij . The edge weight $w : E \rightarrow \mathbb{R}_{\geq 0}$ on G assigns each edge ij a non-negative number w_{ij} . The triple (V, E, w) is called a weighted graph or a metric graph. A path from node a to node b is a collection of edges $e_i = v_i v_{i+1}$ for $i = 0, 1, 2, \dots, n-1$ such that $v_0 = a$ and $v_n = b$. The *length* of the path $\{e_0, e_1, \dots, e_{n-1}\}$ is defined to be $\sum_{i=0}^{n-1} w_{i(i+1)}$. The path is said to have n hops.

A.1 The optimal transport problem

The original optimal transport problem considered by G. Monge in 1781 is to minimize the transportation cost to move iron ores in different mines to a collection of factories which consume the iron ores. Mathematically, the problem is formulated as follows. To begin, let us briefly recall the notion of metric spaces and Borel measures on a metric space. A metric space is a pair (X, d) where X is a set and d is a distance function $d : X \times X \rightarrow \mathbb{R}_{\geq 0}$ with the following properties:

- $d(x, y) = 0$ if and only if $x = y$;
- $d(x, y) = d(y, x)$;
- $d(x, y) + d(y, z) \geq d(x, z)$ for all $x, y, z \in X$.

Given a metric space (X, d) , a Borel set in X is obtained from open sets in X through the operations of countable union, countable intersection, and relative complement. A Borel probability measure μ on a metric space (X, d) assigns each Borel set A a non-negative real number $\mu(A)$ such that

- $\mu(X) = 1$;
- if A_1, \dots, A_n, \dots are disjoint Borel sets then $\mu(\cup_{i=1}^{\infty} A_i) = \sum_{i=1}^{\infty} \mu(A_i)$.

In our case of a finite graph $G = (V, E)$, we take X to be the vertex set V . Every subset of X is Borel. A Borel probability measure can be identified with a function $\mu : V \rightarrow [0, 1]$ such that $\sum_{i \in V} \mu(i) = 1$. Given an edge weighted graph (V, E, w) with $w_{ij} > 0$ for all edges, one introduces a metric d on vertex set V by

$$d(v, v') = \min \left\{ \sum_{i=0}^n w_{k_i, k_{i+1}} : k_i \in V, k_0 = v, k_{n+1} = v', k_i \sim k_{i+1} \right\} \quad (3)$$

where the minimum is taken over all edge paths from v to v' . We call d the induced metric from the edge weight w . Note that by definition, $d(v, v') + d(v', v'') \geq d(v, v'')$ for any three vertices $v, v', v'' \in V$.

Let X and Y be two metric spaces and μ and ν be two probability Borel measures on X and Y respectively. Here X and Y stand for mines and factories and μ and ν are the amount of iron ores to be moved and consumed respectively. Let $c : X \times Y \rightarrow \mathbb{R}_{\geq 0}$ be a continuous function considered as the cost, i.e., the cost of transporting from location x to location y is $c(x, y)$. The function c is usually taken to be the distance $d(x, y)$ if $X = Y$ and the cost of transportation per-unit distance is constant.

A *transport map* $T : (X, \mu) \rightarrow (Y, \nu)$ is a measure preserving map, i.e., for any Borel set $A \subset Y$, $\nu(A) = \mu(T^{-1}(A))$. Monge's formulation of the optimal transportation problem is to find a transport map $T : X \rightarrow Y$ that realizes the infimum

$$\inf \left\{ \int_X c(x, T(x)) d\mu(x) \mid T \text{ is a transportation} \right\}.$$

A map T that attains this infimum (i.e. makes it a minimum instead of an infimum) is called an "optimal transport map". In this generality, there is no mathematical theorem that guarantees the existence of the optimal transportation map. A breakthrough in optimal transportation problem was made by L. Kantorovich in 1942 [60]. In this paper, he formulated the optimal transportation problem as a linear optimization problem whose solution always exists. He replaced the transportation map T by the *transportation plans* which are probability measures γ on the product space $X \times Y$ satisfying $\gamma(A \times Y) = \mu(A)$ and $\gamma(X \times B) = \nu(B)$ for all Borel sets A and B . The goal is to find a transportation plan γ that attains the infimum cost

$$W(\mu, \nu) = \inf \left\{ \int_{X \times Y} c(x, y) d\gamma(x, y) \mid \gamma \in \Gamma(\mu, \nu) \right\},$$

where $\Gamma(\nu, \mu)$ denotes the collection of all transportation plans. If $X = Y$, the quantity $W(\mu, \nu)$ is called the *Wasserstein distance* between two probability measures μ, ν on X . Kantorovich proved that the infimum is always achieved by some transportation plan.

In our case of a finite weighted graph $G = (V, E, w)$ with two probability measures μ and ν on the vertex set V , one can reformulate Kantorovich's problem as follows. Let d be the associated distance function on V defined by Equation (3). A transportation plan γ is given by a map $\gamma : V \times V \rightarrow [0, 1]$ such that $\sum_{i \in V} \gamma_{ij} = \mu_j$ and $\sum_{j \in V} \gamma_{ij} = \nu_i$ for all $i, j \in V$. The goal is to find the minimum cost

$$\min \left\{ \sum_{i, j \in V} \gamma_{ij} d(i, j) : \gamma \text{ is a transportation plan} \right\}.$$

This is a linear programming problem and thus can be computed.

A.2 Curvatures in classical differential geometry

One of the central themes in modern geometry is the notion of curvature which measures how space is curved. It was introduced by Gauss and Riemann over 190 years ago. By an n -dimensional manifold, following Riemann, we mean a space which locally looks like the n -dimensional space. A Riemannian metric on a manifold assigns each tangent space of the manifold a Euclidean metric. Manifolds together with Riemannian metrics, i.e., Riemannian manifolds, are the main objects of study in modern geometry. For instance, a smooth surface in the 3-dimensional Euclidean space is a 2-dimensional Riemannian manifold whose associated Riemannian metric is induced from the 3-dimensional Euclidean space. These are the original objects investigated by Gauss. For such a surface S , the *Gaussian map* from S to the unit sphere sends a point on S to the unit normal vector of S at p . The *curvature* (or Gaussian curvature) of the surface at a point p is the signed area distortion of the Gaussian map at p . To be more precise, it is the Jacobian determinant of the Gaussian map at p . From this definition, one sees that the plane has zero curvature, the sphere has positive curvature, and the hyperboloid of one sheet has negative curvature. Gauss showed (Theorema egregium) that the curvature depends only on the induced Riemannian metric on the surface and does not depend on how the surface is embedded. Riemann generalized Gaussian curvature to high dimensions as follows. For a Riemannian manifold (M, g) , the *sectional curvature* assigns each 2-dimensional linear subspace P in the tangent space $T_p M$ of M at p a scalar (the Riemannian sectional curvature). The scalar is equal to the Gaussian curvature of the image of P under the exponential map. A positively curved space tends to have small diameter and is geometrically crowded (e.g., a sphere). In contrast, a negatively curved space has an infinite fundamental group, a contractible universal cover, and is geometrically spreading out like a tree (in large scale).

The *Ricci curvature* assigns each unit tangent vector v at a point p a scalar which is the average of the sectional curvatures of planes containing v . There are several characteristic properties of the Ricci curvature which are used for defining the Ricci curvature on general metric spaces. Namely, Ricci curvature controls how fast the volume of distance ball grows as a function of the radius. It also controls the volume of the overlap of two balls in terms of their radii and the distance between their centers.

There have been various approaches to generalize the notion of curvature to spaces which are not manifolds (e.g., a graph with edge weights). One of the important work of Ollivier [19] Ricci curvature relates to optimal transport. Since

optimal transport can be formulated on very general metric spaces with probability measure at each point, in particular on networks with edge weights and probability measures at each vertex. This is the approach we take for community detection using curvature and optimal transport.

A.3 Ollivier's work on Ricci curvature for general metric spaces with measures

Ollivier's approach to Ricci curvature relies on the following key theorem [19] which relates curvature with optimal transportation. Let (M^n, d) be an n -dimensional Riemannian manifold with Riemannian distance d whose Ricci curvature is k and Riemannian volume measure is μ . Fix $\varepsilon > 0$, let

$$m_x = \frac{\mu|_{B(x, \varepsilon)}}{\mu(B(x, \varepsilon))} \quad (4)$$

be the probability measure associated to $x \in M$. Then the Wasserstein distance $W(m_x, m_y)$ is

$$(1 - k(x, y))d(x, y), k_{xy} = \frac{\varepsilon^2 k(v, v)}{2(n+2)} + O(\varepsilon^3 + \varepsilon^2 d(x, y))$$

and v is the tangent vector at x of the geodesic xy . This shows that the classical Ricci curvature is related to the optimal transportation problem. This also shows how to define Ricci curvature for general metric spaces with probability measures.

Definition A.1. (Ollivier [19]) Given a metric space (X, d) equipped with a probability measure m_x for each $x \in X$, the Ollivier's Ricci curvature along the shortest path xy is

$$k(x, y) = 1 - \frac{W(m_x, m_y)}{d(x, y)} \quad (5)$$

where $W(m_x, m_y)$ is the Wasserstein distance with respect to the cost function $c(x, y) = d(x, y)$.

A.4 Ricci curvature for weighted graph

In our case of weighted graph, we adapt Ollivier's definition of discrete Ricci curvature and relate it to community detection. On a weighted graph (V, E, w) we consider the associated distance function d defined by Equation (3). To define the Ollivier Ricci curvature, one needs probability measures associated with each vertex. In [57], given a non-negative scalar α , Lin *et al.* defined the probability measure m_x^α on V associated to the vertex $x \in V$ to be

$$m_x^\alpha(i) = \begin{cases} \alpha & \text{if } i = x \\ (1 - \alpha)/|\pi(x)| & \text{if } i \sim x \\ 0 & \text{otherwise,} \end{cases} \quad (6)$$

where $\pi(x)$ is the set of neighbors of x and $|\pi(x)|$ is the number of elements in set. In this work, we extended and generalized the probability distribution defined by Lin *et al.* to further consider the edge weights. The probability measure we constructed is motivated by the classical differential geometry as follows. Consider a network as a discretization of a smooth manifold, a Riemannian metric and a Riemannian distance should correspond to edge weight and distance. Given an edge weighted graph (V, E, w) whose associated distance is d (Equation (3)), we define the associated normalized probability measure (Equation (4)) as follows.

$$m_x^{\alpha, p}(i) = \begin{cases} \alpha & \text{if } i = x \\ \frac{1-\alpha}{C} \cdot \exp(-(d(x, i))^p) & \text{if } i \sim x \\ 0 & \text{otherwise,} \end{cases} \quad (7)$$

where C is a normalization factor $C = \sum_{j \sim x} \exp(-(d(x, j))^p)$. Then the discrete Ricci curvature defined under this mass distribution is as follows:

$$\kappa_{xy} = 1 - \frac{W(m_x^{\alpha, p}, m_y^{\alpha, p})}{d(x, y)} \quad (8)$$

Note that for $p = 0$, the probability measure becomes $m_x^{\alpha, 0}(i) = \frac{1-\alpha}{|\pi(x)|}$ if $i \sim x$, which is the same as Equation (6). For our computation, we take $p = 2$ and $\alpha = 1/2$ in most cases.

To detect the community structure, we introduce a curvature guided diffusion process called discrete Ricci flow (or simply Ricci flow) on a network. The flow was motivated by the powerful tool of smooth Ricci flow which has recently revolutionized the geometry and topology of 3-dimensional spaces. It is also related to the work of discrete Ricci flow on surfaces [47].

The Ricci flow on weighted graph $(V, E, w^{(0)})$ generates a time dependent family of weighted graphs $(V, E, w(t))$ such that the initial value $w(0) = w^{(0)}$ and the weight $w_{ij}(t)$ on edge ij changes proportional to the Ollivier-Ricci curvature $\kappa_{ij}(t)$ at edge ij at time t .

Ollivier, in the future work section of [19], suggested to use the following formula for Ricci flow with continuous time parameter t :

$$\frac{d}{dt}d_{ij}(t) = -\kappa_{ij}(t)d_{ij}(t). \quad (9)$$

In our setting, we use discrete time parameter k and define a discrete Ricci flow as a family of edge weighted graphs $(V, E, w^{(k)})$, $k \in \mathbf{Z}_{\geq 0}$, with associated distances $d^{(k)}$, where $d^{(k)}(i, j)$ is the shortest edge path length between i and j . The flow takes discrete time $k \in \mathbf{Z}_{\geq 0}$.

$$w_{ij}^{(k+1)} = (1 - \kappa_{ij}^{(k)})d^{(k)}(i, j) \quad (10)$$

where $\kappa_{ij}^{(k)}$ is the Ricci curvature at the edge ij of the weighted graph $(V, E, w^{(k)})$. Note that Equation (10) states that $w_{ij}^{(k+1)}$ is equal to the Wasserstein distance between adjacent vertices i and j in the metric graph $(V, E, w^{(k)})$. To detect a community structure on an unweighted graph $G = (V, E)$, we take the initial edge weight $w^{(0)}$ to be the constant 1 and run the Ricci flow (Equation (10)) from there.

The flow tends to expand negatively Ricci curved subgraphs and contract positively Ricci curved subgraphs. In networks with clear community structures, the inter-community edge weights converge to ∞ and the intra-community edge weights converge to 0. Thus the network is naturally partitioned into different communities by removing edges of very high weights. We may continue to run Ricci flow to further partition the communities into smaller ones, when the network has hierarchical community structures. This is similar to the popular Girvan-Newman algorithm [14]. It first computes betweenness centrality for each edge, then removes edges with the highest score. After that, re-compute all scores and repeat. Here the betweenness of an edge is the sum $\sum_{i,j \in V \setminus \{e\}} \frac{\sigma_{ij}(e)}{\sigma_{ij}}$ where σ_{ij} is the number of shortest paths from i to j and $\sigma_{ij}(e)$ is the number of shortest paths from i to j which contain the edge e . Since computing centrality involves global information of the network and is expensive, Ricci flow is easier to implement in practice.

Our work on Ricci curvature on networks builds on our previous work [22] and is also inspired by the important works of E. Saucan and J. Jost *et al.* in [23, 27, 36, 37]. In these works, they systematically introduced and investigated various discrete curvatures for complex networks. The comparative analysis of Forman and Ollivier Ricci curvature on benchmark dataset of complex networks and real-world networks was also carried out. Their numerical results show a striking fact that these two completely different discretization of the Ricci curvatures are highly correlated in many networks.

B From Ricci flow to community detection

In this section, we explain the relationship between the discrete Ricci flow (Equation 10) on networks and the classical theory of 3-manifolds and the Ricci flow. These classical theories motivate us to apply Ricci flow for community detection.

A 3-manifold in mathematics is a connected (Hausdorff) topological space which looks like the 3-space in small scale. More precisely, each point in a 3-manifold has a neighbourhood homeomorphic to an open ball in the 3-space. 3-manifolds are the basic prototypes of 3-dimensional spaces. There are two operations which produce complicated 3-manifolds from simple ones. The first is the connected sum operation and the second is the torus sum. In the connected sum operation, one takes two 3-manifolds, removes two small open balls from them. Glue the two remaining 3-manifolds with holes along their 2-sphere boundary by a homeomorphism. The resulting 3-manifold is the connected sum of the given two. The torus sum operation is similar where one takes two 3-manifolds with torus boundary and glues the two boundary by a homeomorphism. Naturally, one asks if each 3-manifold can be decomposed as a connected sum and torus sum from simple pieces, i.e., reversing the above process. The answer is affirmative and is the content of the classical theorem of topological decomposition of 3-manifolds, established by H. Kneser, J. Milnor [61] Jaco-Shalen [62], and Johannson [63]. The theorem states that each 3-manifold can be canonically decomposed into simple pieces using the 2-spheres and tori. In the sphere decomposition, one looks for topologically essential disjoint

2-spheres in the 3-manifold. Here a topologically essential 2-sphere (or torus) means it is not the boundary of a 3-ball (or a solid torus) in the manifold. By capping off the 2-sphere boundary of the complement by the 3-balls, one obtains new 3-manifolds which have simpler topology and the original 3-manifold is obtained from them by the connected sum. The torus decomposition is similar in construction and uses the essential torus instead of the 2-sphere. A 3-manifold which cannot be decomposed by any essential 2-spheres and tori is called atoroidal. Thus the classical decomposition theorem says that each 3-manifold is a connected sum and torus sum of a collection of atoroidal ones.

One of the most important problems in low-dimensional geometry and topology is the geometrization conjecture proposed by William Thurston in 1976 [64]. It states that any atoroidal 3-manifold admits complete, locally homogeneous Riemannian metrics, i.e., atoroidal 3-manifolds are geometric. This fundamental conjecture was solved by the groundbreaking work of Perelman in 2004 which uses the Ricci flow method developed by R. Hamilton in 1981. A key step in Perelman's proof is that the Ricci flow can detect the 2-sphere and torus decomposition.

The Ricci flow, introduced by Richard S. Hamilton in 1981 [16], deforms the metric of a Riemannian manifold in a way formally analogous to the diffusion of heat, smoothing out irregularities in the metric. Ricci flow has been one of the most powerful tools for solving geometric problems in the past forty years. The flow exhibits many similarities with the heat equation.

Suppose a Riemannian metric g_{ij} is given on a manifold M so that its Ricci curvature is R_{ij} . Then Hamilton's Ricci flow is the following second-order nonlinear partial differential equation on symmetric $(0, 2)$ -tensors:

$$\frac{\partial}{\partial t} g_{ij} = -2R_{ij}.$$

A solution to the Ricci flow is a one-parameter family of metrics $g_{ij}(t)$ on a smooth manifold M satisfying the above partial differential equation. One of the key properties of the Ricci flow is that the curvature evolves according to a nonlinear version of heat equation. Thus the Ricci flow tends to smoothing out irregularity of the curvature.

In the groundbreaking work of G. Perelman, he used the Ricci flow to prove the geometrization conjecture by analyzing the singularity formation and introducing a Ricci flow with 'surgery' [65]. One way a singularity may arise in the Ricci flow is that an essential 2-sphere in the manifold may collapse to a point in finite time. Also essential tori in the manifold can also be detected by the Ricci flow. Thus, one consequence of Perelman's work is that Ricci flow can be used to find the 2-sphere and torus decomposition in a 3-manifold. This is the key motivation for us to introduce a discrete Ricci flow on networks for community detection.

We consider a community structure in a network heuristically to be a discrete counterpart of the (topological) sphere-torus decomposition of a 3-manifold. One can roughly justify this analogy as follows. A commonly agreed characterization of communities in a network is that there are more edges linking nodes within a community and fewer edges linking nodes in different community. This is similar to the components in the sphere decomposition. Indeed, according to the Seifert-van Kampen theorem ([66]), loops within a component in the sphere and torus decomposition interact more among themselves than loops in different components. Since the Ricci flow runs on a manifold with a Riemannian metric and detects topological decompositions, the discrete Ricci flow on a network with edge weight should detect the community structures. This theme has been supported by our numerical experiments.

C Algorithms for discrete Ricci flow on graph

For a given graph $G = (V, E)$, let the edge weight of edge $xy \in E$ be w_{xy} , the discrete Ricci curvature of edge xy , κ_{xy} , is computed as follows:

$$\kappa_{xy} = 1 - \frac{W(m_x^{\alpha,p}, m_y^{\alpha,p})}{d(x, y)},$$

where W is the optimal mass transport distance (a.k.a. Wasserstein Distance or Earth Mover Distance). The mass distribution $m^{\alpha,p}$ is defined as

$$m_x^{\alpha,p}(i) = \begin{cases} \alpha & \text{if } i = x \\ \frac{1-\alpha}{C} \cdot \exp(-(d(x, i))^p) & \text{if } i \sim x \\ 0 & \text{otherwise,} \end{cases}$$

where C is a normalization factor $C = \sum_{j \sim x} \exp(-(d(x, j))^p)$. To speed up the computation of W , we suggest to apply the Sinkhorn distance [67] which computes the approximate optimal transport distance fast without losing too much accuracy.

For discrete Ricci flow computation, we follow Equation 10. For each iteration i , the Ricci flow metric on edge (edge weight) is defined as follows:

$$w_{xy}^{(i+1)} = d^{(i)}(x, y) - \varepsilon \cdot \kappa_{xy}^{(i)} \cdot d^{(i)}(x, y), \quad \forall xy \in E,$$

where ε is the step size or learning rate of the gradient decent process. $d^{(i+1)}(x, y)$ is the shortest path between x and y based on $w^{(i+1)}$.

Since the edge weights change in a relative manner, we re-scale the metric so that the sum of edge weight remains constant. For each iteration, we recompute the Ricci curvature on each edge based on the current edge weight, then update and normalize the weight until $|\kappa_{xy}^{(i)} - \kappa_{xy}^{(i-1)}| < \delta$, where $\delta > 0$. The detailed algorithm is as follows.

Algorithm 1: Discrete Ricci Flow

Input : An undirected graph G and a real number $\delta > 0$.

Output : A weighted graph G with edge weight as Ricci flow metric on each edge.

- 1 Normalize the edge weight $w_{xy}^{(i)} \leftarrow d^{(i)}(x, y) \cdot \frac{|E|}{\sum_{xy \in E} d^{(i)}(x, y)}$
 - 2 Compute the Ricci curvature of G
 - 3 Update the edge weight by $w_{xy}^{(i+1)} \leftarrow d^{(i)}(x, y) - \varepsilon \cdot \kappa_{xy}^{(i)} \cdot d^{(i)}(x, y)$
 - 4 Repeat 1 – 3 until all $|\kappa_{xy}^{(i)} - \kappa_{xy}^{(i-1)}| < \delta$.
-

D Evaluations

Here we briefly introduce these two metrics and apply these metrics to measure the accuracy of our clustering results.

ARI Adjusted Rand Index (ARI) [35] measures the similarity between two clustering results by adjusting the Rand index [68] in a way that a random result gets a score of 0. Suppose the ground truth community is described by a partition of nodes $\{1, 2, \dots, n\}$ into disjoint sets C_1, C_2, \dots, C_m , and the detected community is represented by disjoint sets $\{\bar{C}_1, \bar{C}_2, \dots, \bar{C}_k\}$. ARI scores the agreement of partitioned node pairs in C_i and \bar{C}_j . The ARI of the given clustering result and the actual result is defined as follows.

$$ARI(C, \bar{C}) = \frac{\sum_{i=1}^m \sum_{j=1}^k \binom{|C_i \cap \bar{C}_j|}{2} - [\sum_{i=1}^m \binom{|C_i|}{2}] \sum_{j=1}^k \binom{|\bar{C}_j|}{2} / \binom{|V|}{2}}{\frac{1}{2} [\sum_{i=1}^m \binom{|C_i|}{2} + \sum_{j=1}^k \binom{|\bar{C}_j|}{2}] - [\sum_{i=1}^m \binom{|C_i|}{2}] \sum_{j=1}^k \binom{|\bar{C}_j|}{2} / \binom{|V|}{2}} \quad (11)$$

The value of ARI is 1 when the two clustering results match perfectly and is below 1 otherwise.

Modularity Modularity introduced in [15] describes the fraction of edges between communities minus the expected fraction if edges are distributed uniformly at random. The range of modularity is $[-1, 1]$ where a positive value means more edges are intra-community edges than expected for a random graph. Unlike ARI, Modularity does not require ground truth community, and is easy to compute even for large networks. But modularity suffers from resolution problem due to the statistical nature [69].

For a network G with n node, m edges, c communities and adjacency matrix A , the modularity Q of this network is defined as follows:

$$Q = \frac{1}{(2m)} \sum_{vw} \left[A_{vw} - \frac{k_v k_w}{(2m)} \right] \delta(c_v, c_w) = \sum_{i=1}^c (e_{ii} - a_i^2),$$

where k_x is the degree of node x , $\delta(c_v, c_w)$ equals to 1 if node v and w are in the same community, otherwise 0, and e_{ij} is the fraction of inter-community edges connecting community i and j :

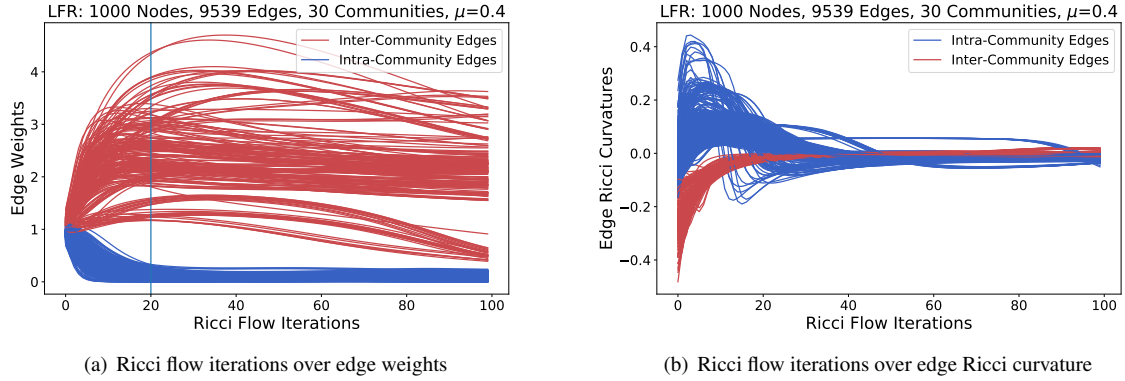
$$e_{ij} = \sum_{vw} \frac{A_{vw}}{2m} 1_{v \in c_i} 1_{w \in c_j},$$

and a_i is the fraction of intra-community edges in community i :

$$a_i = \frac{k_i}{2m} = \sum_j e_{ij}.$$

D.1 Edge Weights under Ricci Flow Iterations

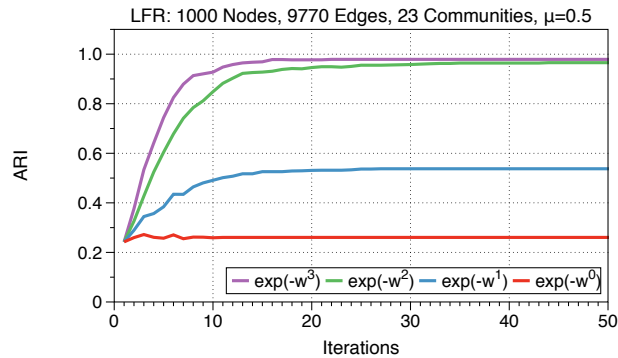
We first analyze the iterating process of Ricci flow on graphs with community structure. In Fig. 9, we showed the variation of edge weights and edge Ricci curvatures on an LFR graph with 1000 nodes and $\mu = 0.4$ with 38 communities and with average degree 20. We name edges to connect nodes in the same community as intra-community edges (labeled as blue) and edges connect nodes in two different communities as inter-community edges (labeled red in the figure). When the iteration process starts, the original weight of all edges is set to be 1 (Fig. 9(a)). As Ricci flow iterates, we can see a clear trend that the weights of intra-community edges (labeled blue in figure) are decreasing and converged to 0 while the weights inter-community edges increased with iterations. In Fig. 9(b), as Ricci flow iterates, the Ricci curvature on all edges converged to a fix value.



Supplementary Figure S 9. Edge weights and Ricci curvatures over Ricci flow iterations on a LFR graph with 1000 nodes, 9539 edges, and $\mu = 0.4$. Fig. 9(a): the edge weights of inter-community edges expand by Ricci flow. Fig. 9(b): edge Ricci curvatures converged to 0 by Ricci flow.

D.2 Ricci Flow Parameters

Here we discuss the influence of different probability measures on Ricci flow. Recall that, when computing the Ricci curvature of each edge, we choose the probability distribution as exponential in the edge weight. This exponential distribution takes *base* to be e and the exponent to be the edge weight to the *power* of p . In Fig. 10, we test the community detection accuracy of Ricci flow using probability distribution with different base and power on LFR graph with 1000 nodes with $\mu = 0.5$ and average degree 20. The result shows that over iterations, choosing $p = 2$ or $p = 3$ yields decent accuracy. Notice that for $p = 0$, the probability distribution is reduced to Lin and Yau's setting [57] that the mass is equally distributed to a node's neighbors during the optimal transportation process.

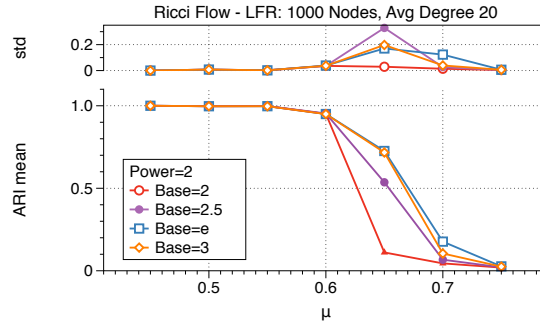


Supplementary Figure S 10. Ricci flow with different power probability measure setting on a LFR graph with 1000 nodes, 9770 edges and $\mu = 0.5$.

In Fig. 11, we check the influence of probability distribution of different *base* with $p = 2$ on LFR graph with 1000 nodes and average degree 20. To eliminate the influence of randomness of the model, for every different μ , we take the

average result over 10 trials. The result shows that for most of the *base* setting, the result is good when μ is smaller than 0.6. For a more mixed graph with greater μ , choose *base* to be *e* yields the most stable result.

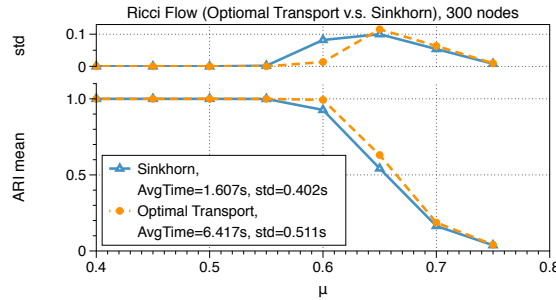
In the following experiments, we stick to *base* = *e* and *power* = 2 as our parameter setting.



Supplementary Figure S 11. Ricci flow with different base probability measure setting on a LFR graph with 1000 nodes, 9770 edges and $\mu = 0.5$.

D.3 Approximated Optimal Transport Distance

To speed up the computation process, we suggest utilizing the Sinkhorn distance [67] as an approximate solution for optimal transport. The result of applying these two distances for Ricci flow is shown in Fig. 12. With regularity term set to be 0.1, the Sinkhorn distance performs equally well as the optimal transport in Ricci flow process. And the time complexity is reduced by four times. The computation time is average over 5 iterations on an Intel(R) Xeon(R) CPU E5-2670 v2 @ 2.50GHz with 512G RAM using 20 processes. Optimal transport is computed by CVXPY(<https://www.cvxpy.org>) with ECOS solver, Sinkhorn distance is solved by POT: Python Optimal Transport(<https://github.com/rflamary/POT>).

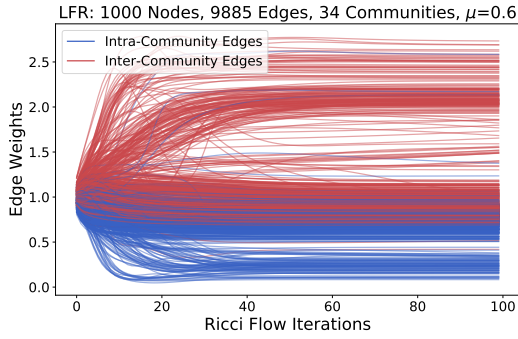


Supplementary Figure S 12. A comparison of applying Sinkhorn distance and optimal transport distance for Ricci flow computations on LFR graph with 300 nodes. The result of applying the Sinkhorn distance is similar as the one using optimal transport while the time cost is four times smaller.

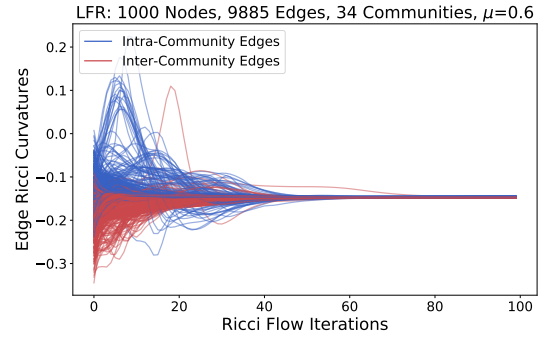
D.4 Ricci flow with Surgery

Without too many parameter settings, Ricci flow yields good clustering performance for the graph with distinct community structures. In more complex graphs especially those with hierarchical community structures, we may need to run Ricci flow multiple times and do surgery during the Ricci flow iterations. For these kinds of graphs, we mimic the surgery process in the classic Ricci flow process during Ricci flow iterations. For every 5 iteration in the Ricci flow process, we cutoff the edges whose weights rank among the top 5%. Fig. 13 presents the edge weight and edge Ricci curvature changes during Ricci flow iterations with surgery. For every 5 iteration, the surgery process cuts out a small part of high weighted edges (mostly inter-community edges), and the surgery helps to further separate the communities. Fig. 14 demonstrates the result of Ricci flow with surgery. With LFR graph of 1000 nodes and $\mu = 0.6$, the surgery process boosts the ARI from 0.3 to 0.8.

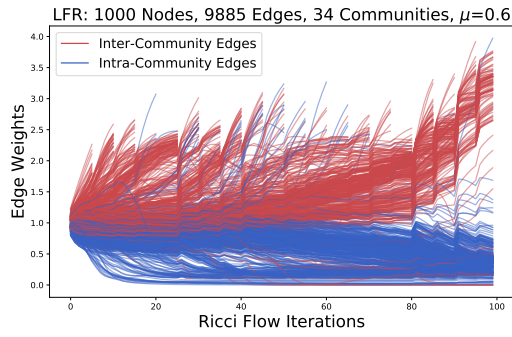
For most of the networks that come without ground-truth community labels, we proposed to use modularity as an index to decide the final edge weight cutoff threshold to detect the communities. For a given graph, we first apply the



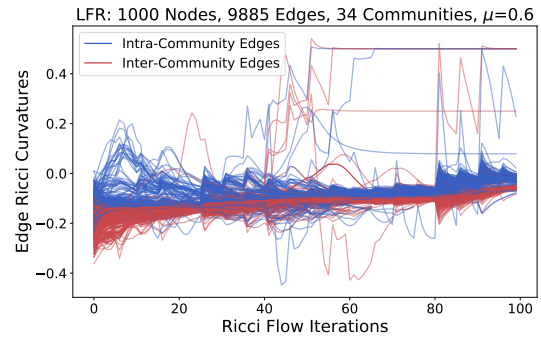
(a) Weight: Without Surgery



(b) Ricci Curvature: Without Surgery

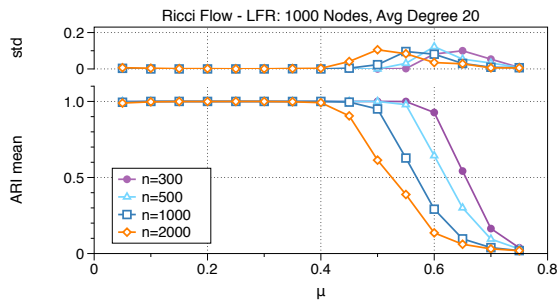


(c) Weight: With Surgery

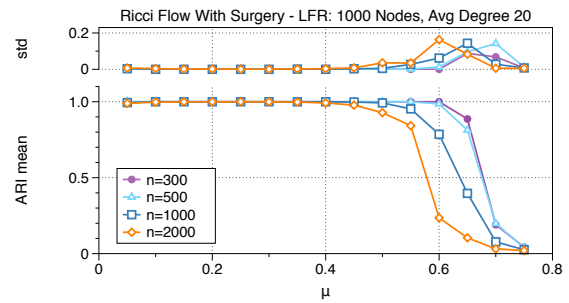


(d) Ricci Curvature: With Surgery

Supplementary Figure S 13. Edge weights and Ricci curvatures over Ricci flow iterations with and without surgery on a LFR graph with 1000 nodes, 9718 edges, and $\mu = 0.6$. In Fig. 13(c) and Fig. 13(d), for every 5 iterations, the surgery process cut out a small part of high weighted edges (mostly inter-community edges). This cutting helps further separate the communities.



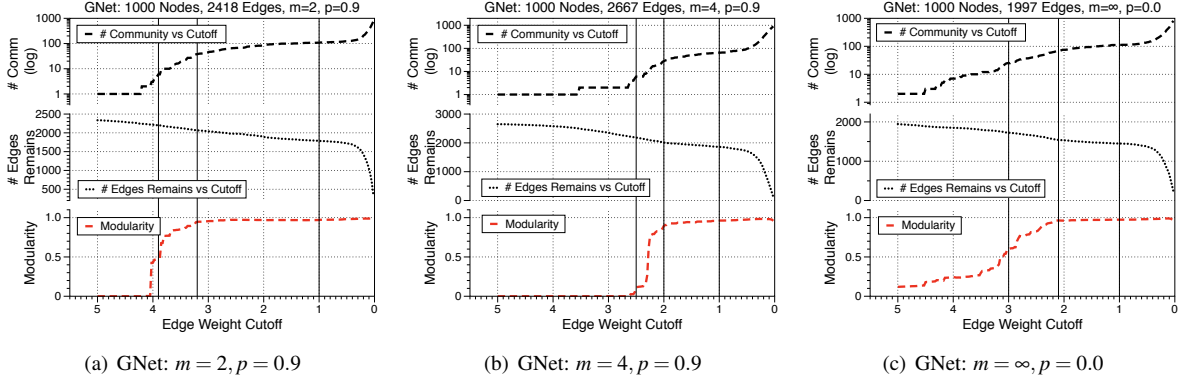
(a) Ricci Flow



(b) Ricci Flow With Surgery

Supplementary Figure S 14. Accuracy evaluation of 50 iterations of Ricci flow and 50 iterations Ricci flow with surgery for every 5 iterations. With LFR graph of 1000 nodes and $\mu = 0.6$, the surgery process boost the clustering accuracy ARI from 0.3 to 0.8.

graph with 20 to 50 iterations of discrete Ricci flow processes. (Iteration required varies by the complexity of the graph. For example, LFR with 1000 nodes in Fig. 13 takes around 50 iterations to fully stabilized.) Then we remove edges from highest to lowest, and log the modularity as Fig. 15. From the relationship of ARI and modularity we observed from Fig. 6 in the main article, we suggest the cutoff threshold to be the point when modularity first hit the plateau of the curve. In Fig. 15 and Fig. 16, we represent three different models of GNet from planar to scale-free to demonstrate the final clustering results with different cutoff thresholds based on modularity. By properly adjusting the cutoff threshold, the hierarchical community structure of the graph is also revealed.



Supplementary Figure S 15. Modularity of GNet with 1000 nodes with different parameter setting. For each setting, we suggest the middle vertical line as cutoff threshold as it is the turning point for modularity curve. We also add two extra cutoff thresholds (left and right vertical line) for comparison. The result of communities detected with these three given cutoff thresholds are shown in Fig. 16.

E Proof of Theorem 4.1

We remark that we are not able to prove the similar result for other Ollivier-Ricci curvatures when $p > 0$ though numerical results indicate it should be true.

We start by computing the Wasserstein distance of a metric on $G(a, b)$. In each community C_i there is a specific node u_i which connects to other communities. We call this node the gateway node and the rest of the nodes in C_i the non-gateway nodes. There are three types of edges in the graph, edges connecting two communities (on two gateway nodes, such as $u_1 u_2$ in Fig. 17), edges connecting a gateway node with a non-gateway node in the same community (such as $u_2 i$ and $u_2 j$), and edges connecting two non-gateway nodes (such as $i j$).

Since the initial metric has edge length one and the Ricci flow preserves the graph symmetry, there are only three different edge lengths at each iteration of the Ricci flow, corresponding to the three types of edges. Suppose the edge lengths of the metric at the n -th iteration are d_1, d_2 and d_3 for the edges between communities, edges from a gateway node to a non-gateway node, and edges between two non-gateway nodes respectively, as shown in Fig. 17. Let edge lengths of the $(n + 1)$ -th iteration be D_1, D_2 and D_3 which are the Wasserstein distances of the corresponding edges for the metric graph $(G(a, b), d)$ with respect to the probability measures $\{\mu_x | x \in V\}$.

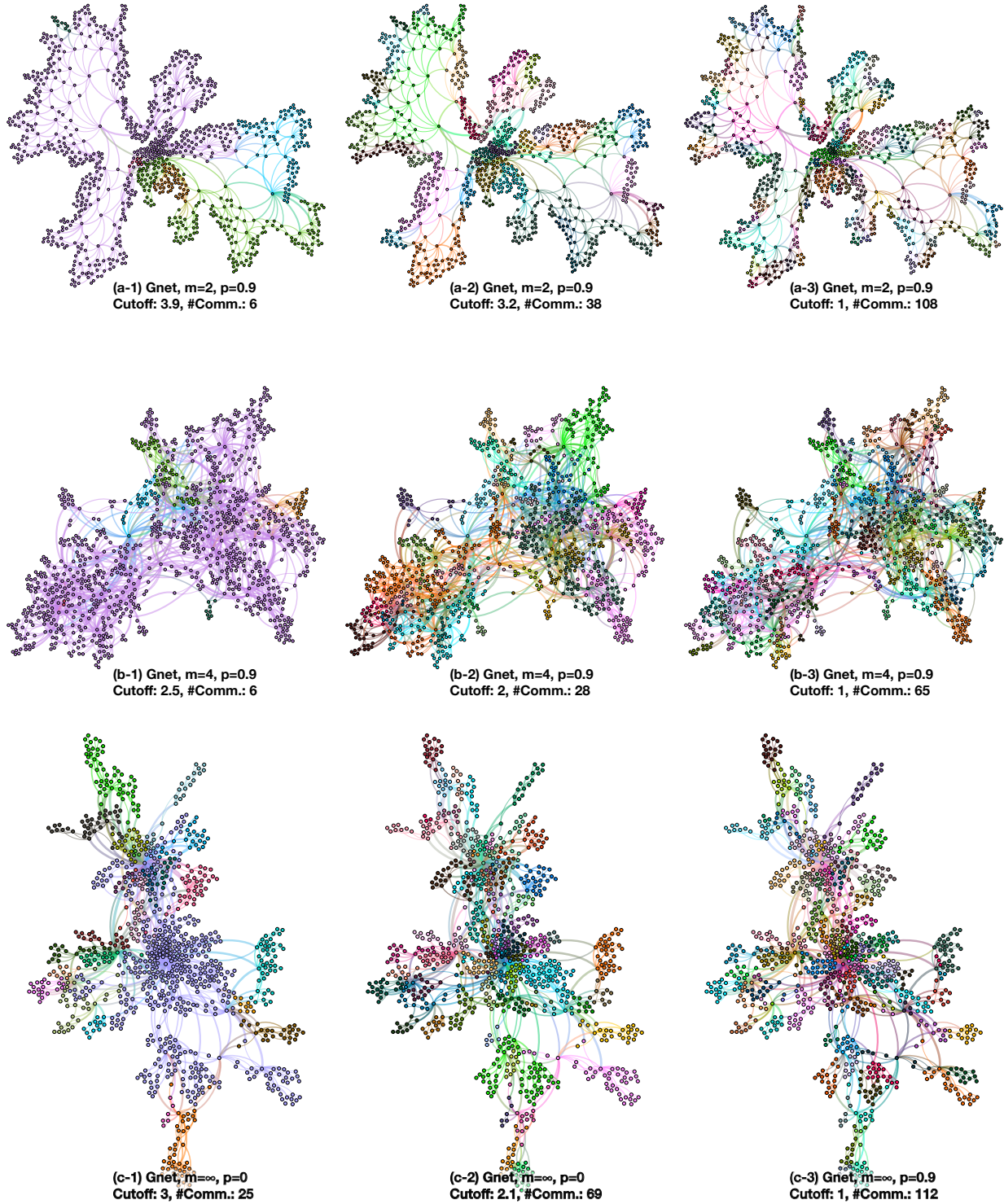
Lemma E.1. The Wasserstein distances D_1, D_2, D_3 are given by

$$\begin{aligned} D_1 &= \frac{a-1}{a+b} d_1 + \frac{2a}{a+b} d_2, \\ D_2 &= \frac{b}{a+b} d_1 + \frac{ab-a-b}{a(a+b)} d_2 + \frac{1}{a+b} d_3, \\ D_3 &= \frac{1}{a} d_3. \end{aligned}$$

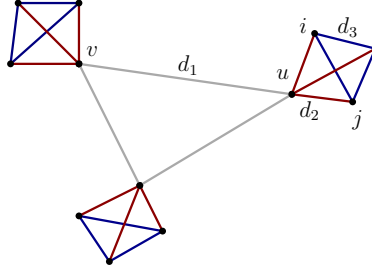
Furthermore, suppose $a > b \geq 2$ and $d_1 \geq d_2 \geq d_3$. Then $D_1 \geq D_2 \geq D_3$.

Proof: The easiest to compute is D_3 . The vertices adjacent to i are the same as vertices adjacent to j . Furthermore, each vertex x adjacent to i (or j) carries the same mass $1/a$. See Fig. 17 (a). Thus the optimal transportation to move μ_i to μ_j is to transport the mass $1/a$ at j to i along the edge ij of distance d_3 . Therefore, $D_3 = \frac{1}{a} d_3$ by definition. See Fig. 2 (a).

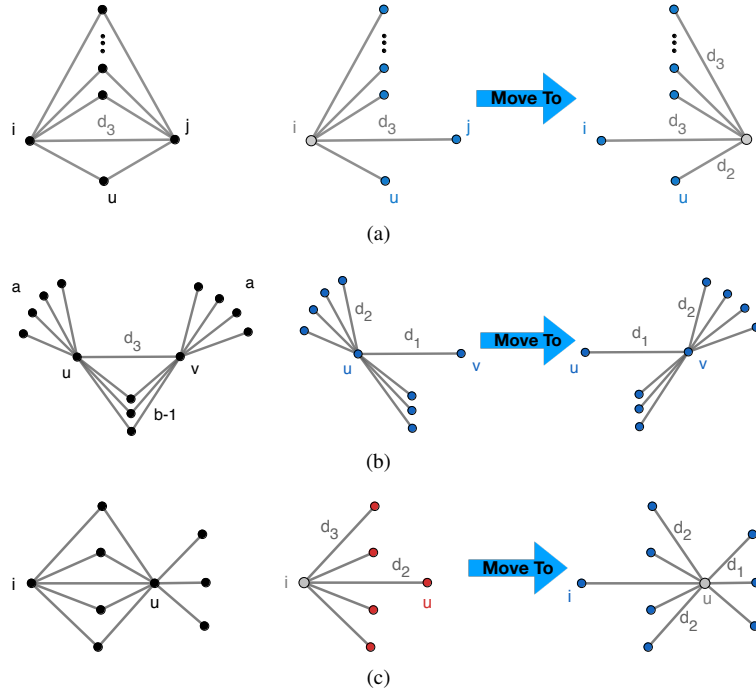
Now let us compute the Wasserstein distance D_1 of moving the probability measures μ_u to μ_v . Note that by definition the vertex degree $d_u = d_v = a + b$. Thus the probability measures μ_u and μ_v have mass $\frac{1}{a+b}$ at vertices adjacent to u or



Supplementary Figure S 16. The emergent geometrical network model generates the following networks: 15(a) a network with random planar geometry for $m = 2$, $p = 0.9$; 15(b) a network with a broad degree distribution, small-world property, and finite spectral dimension for $m = 4$, $p = 0.9$; 15(c) and a scale-free network with power-law degree distribution for $m = \infty$, $p = 0.9$.



Supplementary Figure S 17. The graph $G(a, b)$ obtained from a complete graph on $b + 1$ vertices by replacing each vertex by a complete graph of $a + 1$ vertices. In this figure, $a = 3, b = 2$.



Supplementary Figure S 18. Parts (a), (b) and (c) illustrate the optimal transportation to move the mass at vertex u to vertex v .

v . There are $b - 1$ vertices which are adjacent to both u and v such that each vertex has mass $\frac{1}{a+b}$ in both μ_u and μ_v . Therefore, there is no need to move them. We only need to move the mass $\frac{1}{a+b}$ at each of the rest a many vertices x adjacent to u to those vertices y adjacent to v and need to move the mass at v to the mass at u . The best transportation plan goes as follows.

- Step 1. Move the mass $\frac{1}{a+b}$ at vertex x to u along the edge xu . Since there are a many such vertices x , the total cost is $\frac{a}{a+b}d_2$ where d_2 is the distance from x to u .
- Step 2. Leave a mass of $\frac{1}{a+b}$ at u and move the rest of mass $\frac{a-1}{a+b}$ from u to v along uv . The total cost is $\frac{a-1}{a+b}d_1$.
- Step 3. Finally, move the mass $\frac{a}{a+b}$ at v to vertices y by equal distributions along edges vy of distance d_2 . The total cost is $\frac{a}{a+b}d_2$.

Therefore, $D_1 = \frac{a-1}{a+b}d_1 + \frac{2a}{a+b}d_2$.

Finally, let us compute the Wasserstein distance D_2 of moving the measure μ_i to μ_u . The mass of μ_i at a vertex x adjacent to i is $\frac{1}{a}$ and the mass of μ_u at vertices adjacent to u is $\frac{1}{a+b}$. The best transportation plan is the following. Note that every vertex adjacent to i is also adjacent to u .

- Step 1. Leave the mass $\frac{1}{a+b}$ at each vertex $x \neq u$ adjacent to i . The total leftover mass at these vertices x is $\frac{(a-1)b}{a(a+b)}$. Move

the mass of $\frac{1}{a+b}$ from the leftover mass at these x to the vertex i of distance d_3 from x . The total cost is $\frac{d_3}{a+b}$. After this move, there is a total mass of $\frac{(a-1)b}{a(a+b)} - \frac{1}{a+b} = \frac{ab-a-b}{a(a+b)}$ at these x . Move them to vertex u along edges of length d_2 . The total cost is $\frac{ab-a-b}{a(a+b)}d_2$.

- Step 2. Finally, move a mass of $\frac{b}{a+b}$ at the vertex u to vertices y adjacent to u such that y is not adjacent to i . The total cost is $\frac{bd_1}{a+b}$.

Therefore, the cost of transportation is $D_2 = \frac{d_3}{a+b} + \frac{ab-a-b}{a(a+b)}d_2 + \frac{bd_1}{a+b}$.

Now we come to prove the last statement. Since $d_1 \geq d_2 \geq d_3$, we obtain $D_2 \geq \frac{b}{a+b}d_1 \geq \frac{1}{a}d_1 \geq \frac{1}{a}d_3 = D_3$. Also,

$$\begin{aligned} D_1 - D_2 &= \frac{a(a-b-1)}{a(a+b)}d_1 + \frac{2a^2-ab+a+b}{a(a+b)}d_2 - \frac{a}{a(a+b)}d_3 \\ &\geq \frac{d_2}{a(a+b)}[a(a-b-1) + 2a^2 - ab + a + b - a] \\ &= \frac{d_2}{a(a+b)}[a(a-b-1) + a^2 - ab + a^2 + b] \geq 0. \end{aligned}$$

□

Let A be the 3×3 matrix

$$\begin{bmatrix} \frac{a-1}{a+b} & \frac{2a}{a+b} & 0 \\ \frac{ab-a-b}{a(a+b)} & \frac{1}{a+b} & \frac{1}{a} \\ 0 & 0 & \frac{1}{a} \end{bmatrix}$$

and $W_n = [w_{n1}, w_{n2}, w_{n3}]^t$ be the 3×1 column vector given by $W_{n+1} = AW_n$ with $W_0 = [1, 1, 1]^t$. Then w_{ni} are the edge lengths of the graph $G(a, b)$ after n -th iteration of the Ricci flow. Our goal is to understand the asymptotic behavior of W_n .

Using Maple calculation, we conclude the following lemma.

Lemma E.2. Suppose $a > b \geq 2$, then there are three real eigenvalues $\lambda_1 > \lambda_2 = \frac{1}{a} \geq 0 > \lambda_3$ of the matrix A . The largest eigenvalue $\lambda_1 > \lambda_3$. Furthermore, an eigenvector w_1 associated to λ_1 is of the form $[1, k, 0]^t$ where k is in the open interval $(0, 1)$.

By this lemma, we conclude the proof of the theorem as follows. Let w_2 and w_3 be the eigenvectors associated to λ_1 and λ_3 of A . The $\lambda_2 = \frac{1}{a}$ eigenvector $w_2 = [0, 0, 1]^t$. Since $\lambda_1, \lambda_2, \lambda_3$ are distinct, the eigenvectors w_1, w_2, w_3 are linearly independent in \mathbb{R}^3 .

Write the vector $W_0 = [1, 1, 1]^t = a_1w_1 + a_2w_2 + a_3w_3$. Then using $w_1 = [1, k, 0]^t$ and $\lambda_1 > |\lambda_2|, |\lambda_3|$, we obtain

$$W_n = a_1\lambda_1^n w_1 + a_2\lambda_2^n w_2 + a_3\lambda_3^n w_3 = \begin{bmatrix} a_1\lambda_1^n + o(\lambda_1^n) \\ ka_1\lambda_1^n + o(\lambda_1^n) \\ (\frac{1}{a})^n \end{bmatrix}.$$

Here $o(\lambda_1^n)$ stands for an expression such that $\lim_{n \rightarrow \infty} o(\lambda_1^n)/\lambda_1^n = 0$. As a conclusion, we see that the distance at the edge uv grows at the rate of λ_1^n , the distance at the edges ui and ij grows at rate $o(\lambda_1^n)$. In fact, the distance the edge ij grows at the rate of $\frac{1}{a} < 1$ and shrinks to zero exponentially fast.

References

1. Bhowmick, S. S. & Seah, B. S. Clustering and summarizing protein-protein interaction networks: A survey. *IEEE Trans. Knowl. Data Eng.* **28**, 638–658 (2015).
2. Yang, Z., Algesheimer, R. & Tessone, C. J. A comparative analysis of community detection algorithms on artificial networks. *Sci. Rep.* **6**, 30750 (2016).
3. Fortunato, S. Community detection in graphs. *Phys. Rep.* **486**, 75–174 (2010).

4. Newman, M. E. J. Modularity and community structure in networks. *Proc. Natl. Acad. Sci. U. S. A.* **103**, 8577–8582 (2006).
5. Sinha, A., Gleich, D. F. & Ramani, K. Gauss's law for networks directly reveals community boundaries. *Sci. Rep.* **8**, 11909 (2018).
6. Leskovec, J., Lang, K. J. & Mahoney, M. Empirical comparison of algorithms for network community detection. In *Proc. 19th Int. Conf. World Wide Web*, 631–640 (ACM, 2010).
7. Clauset, A., Newman, M. E. J. & Moore, C. Finding community structure in very large networks. *Phys. Rev. E* **70**, 066111 (2004).
8. Zhang, P. & Moore, C. Scalable detection of statistically significant communities and hierarchies, using message passing for modularity. *Proc. Natl. Acad. Sci.* **111**, 18144–18149 (2014).
9. Peel, L., Larremore, D. B. & Clauset, A. The ground truth about metadata and community detection in networks. *Sci. Adv.* **3**, e1602548 (2017).
10. Allen, B. *et al.* Evolutionary dynamics on any population structure. *Nature* **544**, 227–230 (2017).
11. Abbe, E. Community detection and stochastic block models: Recent developments. *J. Mach. Learn. Res.* **18**, 1–86 (2018).
12. Raghavan, U. N., Albert, R. & Kumara, S. Near linear time algorithm to detect community structures in large-scale networks. *Phys. Rev. E Stat. Nonlin. Soft Matter Phys.* **76**, 036106 (2007).
13. Rosvall, M. & Bergstrom, C. T. Maps of random walks on complex networks reveal community structure. *Proc. Natl. Acad. Sci. U. S. A.* **105**, 1118–1123 (2008).
14. Girvan, M. & Newman, M. E. J. Community structure in social and biological networks. *Proc. Natl. Acad. Sci. U. S. A.* **99**, 7821–7826 (2002).
15. Newman, M. E. & Girvan, M. Finding and evaluating community structure in networks. *Phys. Rev. E* **69**, 026113 (2004).
16. Hamilton, R. S. Three-manifolds with positive ricci curvature. *J. Differ. Geom.* **17**, 255–306 (1982).
17. Perelman, G. The entropy formula for the ricci flow and its geometric applications. (2002). <https://arxiv.org/abs/math/0211159>.
18. Jost, J. *Riemannian geometry and geometric analysis* (Springer Science & Business Media, 2011).
19. Ollivier, Y. Ricci curvature of markov chains on metric spaces. *J. Funct. Anal.* **256**, 810–864 (2009).
20. Ollivier, Y. A survey of ricci curvature for metric spaces and markov chains. In *Probabilistic Approach to Geometry*, 343–381 (Math. Soc. of Japan, Tokyo, Japan, 2010). <https://doi.org/10.2969/aspm/05710343>.
21. Lott, J. & Villani, C. Ricci curvature for metric-measure spaces via optimal transport. *Annals Math. Second. Ser.* **169**, 903–991 (2009).
22. Ni, C.-C., Lin, Y.-Y., Gao, J., Gu, X. D. & Saucan, E. Ricci curvature of the internet topology. In *IEEE. Ic. Comp. Com. Net. (INFOCOM)*, vol. 26, 2758–2766 (IEEE, 2015). <https://doi.org/10.1109/INFOCOM.2015.7218668>.
23. Samal, A. *et al.* Comparative analysis of two discretizations of Ricci curvature for complex networks. *Sci. Rep.* **8**, 8650 (2018).
24. Sreejith, R. P., Mohanraj, K., Jost, J., Saucan, E. & Samal, A. Forman curvature for complex networks. *J. Stat. Mech: Theory Exp.* **2016**, 063206 (2016).
25. Wang, C., Jonckheere, E. & Banirazi, R. Wireless network capacity versus Ollivier-Ricci curvature under Heat-Diffusion (HD) protocol. In *2014 American Control Conference*, 3536–3541 (IEEE, 2014).

26. Whidden, C. & Matsen, F. A. Ricci–Ollivier curvature of the rooted phylogenetic subtree–prune– regraft graph. *Theor. Comput. Sci.* **699**, 1–20 (2017).
27. Jost, J. & Liu, S. Ollivier’s Ricci curvature, local clustering and Curvature-Dimension inequalities on graphs. *Discret. Comput. Geom.* **51**, 300–322 (2014).
28. Sandhu, R. *et al.* Graph curvature for differentiating cancer networks. *Sci. Rep.* **5**, 12323 (2015).
29. Sandhu, R. S., Georgiou, T. T. & Tannenbaum, A. R. Ricci curvature: An economic indicator for market fragility and systemic risk. *Sci Adv* **2**, e1501495 (2016).
30. Ni, C.-C., Lin, Y.-Y., Gao, J. & Gu, X. Network alignment by discrete Ollivier-Ricci flow. In *Graph Drawing and Network Visualization*, 447–462 (Springer International Publishing, 2018).
31. Bastian, M., Heymann, S. & Jacomy, M. Gephi: An open source software for exploring and manipulating networks. *Int. AAAI Conf. on Weblogs Soc. Media* (2009).
32. Lancichinetti, A., Fortunato, S. & Radicchi, F. Benchmark graphs for testing community detection algorithms. *Phys. Rev. E* **78**, 046110 (2008).
33. Bianconi, G., Darst, R. K., Iacovacci, J. & Fortunato, S. Triadic closure as a basic generating mechanism of communities in complex networks. *Phys. Rev. E Stat. Nonlin. Soft Matter Phys.* **90**, 042806 (2014).
34. Wu, Z., Menichetti, G., Rahmede, C. & Bianconi, G. Emergent complex network geometry. *Sci. reports* **5**, 10073 (2015).
35. Hubert, L. & Arabie, P. Comparing partitions. *J. Classif.* **2**, 193–218 (1985).
36. Saucan, E., Samal, A., Weber, M. & Jost, J. Discrete curvatures and network analysis. *MATCH Commun. Math. Comput. Chem.* **80**, 605–622 (2018).
37. Sreejith, R. P., Jost, J., Saucan, E. & Samal, A. Systematic evaluation of a new combinatorial curvature for complex networks. *Chaos Solitons Fractals* **101**, 50–67 (2017).
38. Bakry, D. & Émery, M. Diffusions hypercontractives. In Azéma, J. & Yor, M. (eds.) *Séminaire de Probabilités XIX 1983/84*, vol. 1123 of *Lecture Notes in Mathematics*, 177–206 (Springer Berlin Heidelberg, Berlin, Heidelberg, 1985).
39. Bonciocat, A. I. & Sturm, K. T. Mass transportation and rough curvature bounds for discrete spaces. *J. Funct. Anal.* (2009).
40. Bonciocat, A.-I. A rough curvature-dimension condition for metric measure spaces. *Cent. Eur. J. Math.* **12**, 362–380 (2014).
41. Wang, C., Jonckheere, E. & Banirazi, R. Interference constrained network control based on curvature. In *Proc. American Control Conference*, vol. 2016-July, 6036–6041 (IEEE, 2016).
42. Pal, S. *et al.* Jaccard curvature—an efficient proxy for Ollivier-Ricci curvature in graphs. In *Complex Networks IX*, 51–63 (Springer International Publishing, 2018).
43. Forman, R. Bochner’s method for cell complexes and combinatorial ricci curvature. *Discret. Comput. Geom.* **29**, 323–374 (2003).
44. Weber, M., Saucan, E. & Jost, J. Characterizing complex networks with Forman-Ricci curvature and associated geometric flows. *J Complex Netw* **5**, 527–550 (2017).
45. Weber, M., Jost, J. & Saucan, E. Detecting the coarse geometry of networks. In *NeurIPS 2018 Workshop* (2018). https://www.mis.mpg.de/preprints/2018/preprint2018_97.pdf.
46. Saucan, E., Wolansky, G., Appleboim, E. & Zeevi, Y. Y. Combinatorial ricci curvature and laplacians for image processing. In *2nd Int. Cong. on Image and Signal Processing*, 1–6 (2009). <https://doi.org/10.1109/CISP.2009.5304710>.

47. Chow, B., Luo, F. *et al.* Combinatorial Ricci flows on surfaces. *J. Differ. Geom.* **63**, 97–129 (2003).
48. Plantié, M. & Crampes, M. Survey on social community detection. In *Social Media Retrieval*, Computer Communications and Networks, 65–85 (Springer, London, 2013).
49. Parés, F. *et al.* Fluid communities: A competitive, scalable and diverse community detection algorithm. In *Complex Networks & Their Applications VI*, 229–240 (Springer International Publishing, 2018).
50. Yin, H., Benson, A. R., Leskovec, J. & Gleich, D. F. Local higher-order graph clustering. *ACM Trans. on Knowl. Discov. from Data (TKDD)* **2017**, 555–564 (2017).
51. Newman, M. E. J. Equivalence between modularity optimization and maximum likelihood methods for community detection. *Phys. Rev. E* **94**, 052315 (2016).
52. Decelle, A., Krzakala, F., Moore, C. & Zdeborová, L. Asymptotic analysis of the stochastic block model for modular networks and its algorithmic applications. *Phys. Rev. E* **84**, 066106 (2011).
53. Ji, J., Zhang, A., Liu, C., Quan, X. & Liu, Z. Survey: Functional module detection from protein-protein interaction networks. *IEEE Trans. Knowl. Data Eng.* **26**, 261–277 (2014).
54. Reichardt, J. & Bornholdt, S. Statistical mechanics of community detection. *Phys. Rev. E* **74**, 016110 (2006).
55. Faqeeh, A., Osat, S. & Radicchi, F. Characterizing the analogy between hyperbolic embedding and community structure of complex networks. *Phys. Rev. Lett.* **121**, 098301 (2018).
56. Salnikov, V., Cassese, D. & Lambiotte, R. Simplicial complexes and complex systems. *Eur. J. Phys.* **40**, 014001 (2018).
57. Lin, Y., Lu, L. & Yau, S.-T. Ricci curvature of graphs. *Tohoku Math. J.* **63**, 605–627 (2011).
58. Kunegis, J. KONECT: The koblenz network collection. In *Proceedings of the 22Nd International Conference on World Wide Web, WWW '13 Companion*, 1343–1350 (ACM, New York, NY, USA, 2013).
59. Leskovec, J. & Krevl, A. SNAP Datasets: Stanford large network dataset collection. <http://snap.stanford.edu/data> (2014).
60. Kantorovich, L. V. On the translocation of masses. In *Dokl. Akad. Nauk. USSR (NS)*, vol. 37, 199–201 (1942).
61. Milnor, J. A unique decomposition theorem for 3-manifolds. *Amer. J. Math.* **84**, 1–7 (1962).
62. Jaco, W. & Shalen, P. B. SEIFERT FIBERED SPACES IN 3-MANIFOLDS. In Cantrell, J. C. (ed.) *Geometric Topology*, 91–99 (Academic Press, 1979).
63. Johannson, K. *Homotopy Equivalences of 3-Manifolds with Boundaries* (Springer, 2006).
64. Thurston, W. P. Three dimensional manifolds, kleinian groups and hyperbolic geometry. *Bull. Am. Math. Soc.* **6**, 357–382 (1982).
65. Morgan, G., John; Tian. Ricci flow and the poincaré conjecture. *Clay Math. Monogr.* **3**, 521 (2007).
66. Spanier, E. H. Algebraic topology. (1966).
67. Cuturi, M. Sinkhorn distances: Lightspeed computation of optimal transport. In Burges, C. J. C., Bottou, L., Welling, M., Ghahramani, Z. & Weinberger, K. Q. (eds.) *Advances in Neural Information Processing Systems 26*, 2292–2300 (Curran Associates, Inc., 2013).
68. Rand, W. M. Objective criteria for the evaluation of clustering methods. *J. Am. Stat. association* **66**, 846–850 (1971).
69. Fortunato, S. & Barthélemy, M. Resolution limit in community detection. *Proc. Natl. Acad. Sci. U. S. A.* **104**, 36–41 (2007).